

<https://doi.org/10.1590/2318-0331.272220220092>

LiDAR data for topographical and river drainage characterization: capabilities and shortcomings

Dados LiDAR para caracterização topográfica e de redes de drenagem: potencialidades e limitações

Rafael Lopes Mendonça¹  & Adriano Rolim da Paz^{1*} 

¹Universidade Federal da Paraíba, João Pessoa, PB, Brasil

E-mails: rafaello.mendonca@gmail.com (RLM), adrianorpaz@yahoo.com.br (ARP)

Received: September 21, 2022 - Revised: November 17, 2022 - Accepted: November 19, 2022

ABSTRACT

Topographic data is increasingly available from LiDAR (Light Detection and Ranging) surveys. This research evaluates the limitations and capabilities of a LiDAR Digital Terrain Model (DTM) regarding catchment topography representation and river drainage network derivation, considering high-resolution (1 m) and resampled versions (2, 5, 10, and 30 m), and the Garças river basin (4,100 km²; Pernambuco state) as a study case. The terrain representation of the 1m-DTM and the derived network present outstanding quality, and its coarsening up to 30m resolution still outperforms the results obtained with SRTM data. LiDAR DTM coarsened to 2, 5, 10 and 30 m led to river length shortening of 0.1%, 0.3%, 1.2%, and 4%, respectively, while the difference between LiDAR 1m and SRTM was about 12%. The computational cost for 1m-DTM processing was prohibitive when using a typical low-cost computer, while some algorithms proved to be largely efficient (100 times faster) when running on a more powerful machine. DTM coarsening is an alternative to achieving a better balance between data quality and computer requirements.

Keywords: Digital terrain model; Resampling; Flow directions; Digital elevation model; Computational cost.

RESUMO

Dados topográficos de levantamentos LiDAR (Light Detection and Ranging) estão disponíveis de forma crescente. Esta pesquisa avalia limitações e potencialidades de um Modelo Digital do Terreno (MDT) LiDAR para representação topográfica de bacias hidrográficas e extração de rede de drenagem, considerando alta resolução espacial (1 m) e versões reamostradas (2, 5, 10 e 30 m) e a bacia do rio das Garças (4.100 km²; Pernambuco) como estudo de caso. A representação do terreno com o MDT de 1m e a rede de drenagem apresentam excelente qualidade, e a reamostragem para até 30 m supera o obtido com dados SRTM. O MDT LiDAR reamostrado para 2, 5, 10 e 30 m levou a encurtamentos do rio principal de 0,1%, 0,3%, 1,2% e 4%, respectivamente, enquanto a diferença entre LiDAR 1m e SRTM foi de 12%. O custo computacional para processar MDT de 1m foi proibitivo ao usar computador comum de baixo custo, enquanto alguns algoritmos mostraram-se muito eficientes (até 100x mais rápido) quando rodados em máquina mais robusta. A reamostragem do MDT é um meio de equilibrar qualidade da informação e exigências computacionais.

Palavras-chave: Modelo digital do terreno; Reamostragem; Direções de fluxo; Modelo digital de elevação; Custo computacional.

INTRODUCTION

Several products derived from RS (Remote Sensing) surveys are increasingly available for environmental studies and such information has shown to be extremely valuable for spatio-temporal assessment (e.g. Lecours et al., 2017; Murray et al., 2018; Pettorelli et al., 2018; Klein et al., 2021). That is due to several advantages of RS data, including easiness and velocity to obtain and share, free availability for part of them, standardization (which makes possible an easy way to develop and adjust computational tools for processing them), quality control, spatial coverage, availability for large areas (Smith & Clark, 2005). In addition, there is continuous improvement in the diversity, quantity, and quality of this type of data, including new satellites, airborne platforms, and even on-ground monitoring (McCabe et al., 2017).

The topographic characterization represents important data for several environmental studies. The relief plays a key role in several environmental characteristics, aspects, and processes, including those related to hydrology, erosion and sediment transport, nutrient cycling, species richness and distribution, pollutant dispersal, and site selection for solar and wind energy (Mukherjee et al., 2013).

For hydrology, topographic data acquired by RS and made available as DEM (Digital Elevation Models) is crucial in developing water resources projects and also for supporting scientific advances. The availability of DEM helps the planning, monitoring, and modeling of critical regions, including, for example, flooding areas (Sanders, 2007; Maidment, 2017) and landslides (Schulz et al., 2017). DEMs are also input data for locating areas that carry pollutants to a river (Xiang et al., 2020), to simulate the effects of land use land cover change on runoff (Munoth & Goyal, 2019), to estimate hydrological and geomorphological properties of a region (Sofia et al., 2014), including soil moisture, soil stability, rain retention, runoff erosion (Li, 2009), to flow and sediment transport analysis (Syvitski & Milliman, 2007); and to estimate the extent and timing of floods (Jamali et al., 2018), among others.

One of the major uses of DEM in hydrology is to automatically derive and characterize river drainage networks, besides the use to extracting geomorphological information needed for several studies such as hydrological modeling (Choi et al., 2011; Barnes et al., 2014a; Takaku et al., 2014; Riegler et al., 2015).

In this sense, the DEM provided by SRTM (Shuttle Radar Topography Mission) since 2000 (Farr et al., 2007) may be considered a landmark given its scope, relative quality, and gratuity. It is considered a precursor and still today the main source of global free topographic RS data (Paz & Collischonn, 2008; Buarque et al., 2009; Schumann & Bates, 2018). Initially globally available with 90 m spatial resolution and further released with 30 m spatial resolution, it opened the possibilities and dropped traditional barriers regarding the free, global access to topographic data, providing a way to rapidly develop studies for large areas, including those with difficult access to.

Several other Remote Sensing based DEMs have been freely available since then, such as the ASTER GDEM (Advanced Spaceborne Thermal Emission and Reflection Radiometer, Global Digital Elevation Model) (Tachikawa et al., 2011), the ALOS AW3D (Advanced Land Observing Satellite, World 3D-Digital Elevation Model) (Tadono et al., 2015), the ALOS PALSAR

DEM-ALOS (Phased Array type L-band Synthetic Aperture Radar Digital Elevation Model) (Ngula Niipele & Chen, 2019) and the TanDEM-X World DEM (TerraSAR-X add-on for Digital Elevation Measurement) (Krieger et al., 2007).

However, there are some implications when using these RS topographic data. For instance, the SRTM mission presents absolute and relative elevation errors of 16 and 6 m, respectively (Schumann & Bates, 2018). In other words, depending on the size of the study area and the level of precision required, the use of this data becomes unviable, due to the coarse spatial resolution and the relatively low accuracy of the altimetry. Efforts have been conducted to improve previously released data, by removing vegetation or built/artificial features and other types of noises, such as Bare-Earth DEM (O'Loughlin et al., 2016), Earth-Env (Earth-Environment) DEM (Robinson et al., 2014), MERIT DEM (Multi-Error-Removed Improved-Terrain; Yamazaki et al., 2019), Copernicus DEM (Li et al., 2022), and FABDEM (Forest And Buildings removed Copernicus DEM; (Hawker et al., 2022). However, whilst such derived versions are widely used, they still typically exhibit vertical errors much larger than those acceptable for some applications, including on local scale applications (Schumann & Bates, 2018).

On another development front, there is the increasing availability of topographic data acquired through LiDAR (Light Detection and Ranging) surveys. LiDAR can be defined as a remote sensor system for acquiring, at least, planialtimetric coordinates of targets on the surface (Lillesand et al., 2015). The LiDAR data allows representation of the catchment relief in an unprecedented way, as pointed out by studies such as Murphy et al. (2008) and Persendt & Gomez (2016), which compared LiDAR-derived topography with other data sources, e.g. globally available DEM and aerial orthophotographs. This better topography representation provides the basis for deriving river drainage networks with detail not ever imagined a few decades ago, and such improvement is illustrated by several recent studies (Lindsay & Dhun, 2015; Du et al., 2017; Roelens et al., 2018). Improving the quality of river drainage network characteristics such as length, slope, sinuosity, and positioning of flow paths and river junctions helps to boost hydrological modeling. For instance, errors in river length difficult the model to adequately represent propagation time and accurately attenuate flood waves (e.g. Gandolfi & Bischetti, 1997; Olivera & Raina, 2003; Wu et al., 2008; Lindsay & Evans, 2008; Gironás et al., 2010; Lauri & Kumm, 2014). Errors in river positioning may cause the model to misrepresent tributaries contribution and also the location of floodplain inundation thus affecting flow routing and flood extent simulation (e.g. Getirana et al., 2009).

The inaccurate representation of measured river drainage networks has also a strong influence on modeling studies comparing water availability and water demand (Döll & Lehner, 2002) as well as studies simulating fine-scale exchange between surface water and groundwater, wider patterns on groundwater recharge/discharge, and riparian groundwater (Käser et al., 2014). Overland flow paths upstream from the river drainage networks are also important to be represented as accurate as possible in hydrological models, as it may affect simulating streamflow generation (Giannoni et al., 2005), sediment and pollutant transport to streams (Mayorga et al., 2005; Duke et al., 2006; Yamazaki et al., 2009), spatial and

temporal variations on flow velocities (Piégay et al., 2008), and spatial distribution of soil moisture (Kenward, 2000; Raaflaub & Collins, 2006).

In summary, better-representing overland and river flow paths in hydrological models reduce the propagation of errors through the model structure, reduces the compensation effect achieved by model calibration, and contributes to obtaining a more physically based model (Sousa & Paz, 2017), which is in agreement to the best practices recommended for hydrologic modeling (e.g. Semenova & Beven, 2015).

Despite being useful for improving topography and river drainage network representation, the use of LiDAR data may be challenging due to its computational cost, once in a short period, the DTM went from a spatial resolution of 30-90 m to sub-metric, with billions of pixels (Barnes, 2017). This requires an increase in computational power and storage and improvement of the algorithms used to process this data (Zhu et al., 2006; Gong & Xie, 2009; Barnes et al., 2014b; Yıldırım et al., 2015; Stanislawski et al., 2018). Those methods have to be able to treat flat areas (Barnes et al., 2014a), remove depressions (Lindsay & Dhun, 2015), and determine flow accumulation (Zhou et al., 2019) for so refined and large amount of data.

Another issue is related to adequately understanding and evaluating the quality of derived drainage networks, as so fine-resolution data may present an excess of information related to fine details of the networks. In this sense, due to this level of detail of the surface under study, even the smallest elements detected by the sensor system or even the smallest noises can cause major changes in the determination of the drainage network. This has led some authors to coarsen the original spatial resolution of LiDAR DTM (Gökgöz & Baker, 2015; Moretti & Orlandini, 2018) or to use smoothing techniques (Erdrügger et al., 2021). Studies like Lindsay et al. (2019) claim that fine-resolution LiDAR data often have an excessive surface roughness that can make it difficult to characterize the topographic shape and this implies errors in automated extraction drainage networks.

In this sense, this paper aims to analyze the limitations and capabilities of the use of LiDAR DTM for the topographic characterization of watersheds and extraction of drainage networks. Initially, a compilation of the main concepts and fundamentals of LiDAR is presented, which serves as a beacon of knowledge for further LiDAR users in the water resources field, helping them to critically analyze their data and results. Then, a tributary of the Garças River, in the state of Pernambuco, is chosen as the study case, taking advantage of the availability of LiDAR data from the PE3D project (Pernambuco Tridimensional; Cirilo et al., 2015). Within this study case, a fourfold purpose is addressed: (i) to analyze the ability of LiDAR DTM to represent the bare earth surface, relating it to land use and land cover; (ii) to overall assess the quality of the drainage network derived from the LiDAR DTM and the corresponding effect of spatial resolution coarsening; (iii) to compare the quality of these LiDAR DTM-derived river networks to the results obtained from SRTM DEM; (iv) to evaluate the computational performance of distinct algorithms for depression removal and flow accumulation determination from LiDAR DTM.

LIDAR TECHNOLOGY

LiDAR can be defined as a remote sensor system for acquiring planialtimetric coordinates (x , y , and z) of targets (Lillesand et al., 2015). The altitude measurement (z) is based on the time interval between the emission and reception of the laser signal, and the LiDAR is classified as an active remote sensor, as it does not depend on an external light source for its operation, using its laser as a light source for data acquisition (Novo, 2010; Dong & Chen, 2018; Bigdeli et al., 2018).

LiDAR is treated as a sensor system, for using a set of equipment, in addition to the laser, to obtain the point cloud with planialtimetric coordinates. The LiDAR remote sensing system consists mainly of (1) a laser signal emitter and receiver, which obtains the altimetric coordinate (z coordinate) of the target; (2) a GNSS (Global Navigation Satellite System) positioning system, for measuring x and y coordinates; (3) and an IMU (Inertial Measurement Unit), which measures the angles (ω , ϕ , κ) of altitude (roll, pitch, and yaw) of the aerial or orbital platform; (4) a robust data storage system and, in some cases, a camera can be integrated (Lillesand et al., 2015; Dong & Chen, 2018).

There are three major types of LiDAR systems according to the location of the platform used to install the sensor system: (1) aerial, if the platform is an aircraft, also called ALS (Airborne Laser Scanning); (2) orbital or satellite, if the platform is a satellite; (3) terrestrial, when the sensor system is installed on tripod support, automobile or any other platform that is in contact with the ground. Because it is in contact with the ground, the terrestrial LiDAR sensor system does not require the measurement of altitude angles and therefore dispenses with the IMU. Another aspect of using terrestrial laser scanning is that data collection can be static, from a fixed reference point in the study area, or kinematic/mobile, using a moving platform (Dong & Chen, 2018).

The data from these systems are post-processed to establish the correlations, the filtering of noise, and overlapping points. A single laser pulse when intercepting objects along the path returns to the sensor system as data to be processed and which is present in the point cloud resulting from the survey. The result is the cloud of three-dimensional points of the terrain referring to the first return, intermediate returns, and last return of the same laser pulse (Jensen & Epiphonio, 2011; Dong & Chen, 2018). The existence of multiple returns represents one of the unique characteristics of the LiDAR system, and which enable to generate the DTM (Digital Terrain Model) and the DSM (Digital Surface Model). The first one represents the natural terrain while the latter represents both the natural and built/artificial features of the environment.

The points relative to the bare surface, or exposed soil, are the points referring to the DTM. Such points can be represented on the first or last return, depending on the path taken by the laser pulse and the existence of objects on the bare surface. While for DSM, all points of the survey are considered, not only those that represent the exposed soil.

The point cloud obtained by this system is extremely dense and corresponds to a three-dimensional point sample of the surface. The density of points varies according to survey parameters, the sensor, system, and the platform used, being normally up to 25 points per m^2 (Höfle & Rutzinger, 2011) and up to 50 points per

m² for steep or densely vegetated regions (Lillesand et al., 2015). The density can be expressed as the distance between the laser pulses and depends on: (1) the altitude; (2) aircraft speed; (3) the scanning angle; (4) and the scan rate (Lillesand et al., 2015). When planning the survey with a LiDAR sensor, the overlapping of the scan lines should be provided, to avoid data gaps. The regions that do not have data are called data voids (Jensen & Epiphany, 2011). The recommended overlap is 30 to 50%, depending on the study area, having a direct proportion to the slope of the land and the amount of vegetation cover (Jensen, 2009). Steep or vegetated areas generally require a smaller scanning system opening angle, which results in a denser point cloud (Lillesand et al., 2015).

The accuracy of LiDAR data is measured by surveying the coordinates of control points with high-precision equipment (geodetic GNSS or using a total station, for example). The precision obtained by this equipment and its techniques may be millimetric (Zhang et al., 2021).

The LiDAR survey has been useful for several distinct purposes. The laser pulse of LiDAR can penetrate the trees' canopy and this special characteristic increases the frequency of using LiDAR in forestry applications (Bigdeli et al., 2018; Torre-Tojal et al., 2022), such as: estimating volume and biomass (van Leeuwen & Nieuwenhuis, 2010), tree height (Wang & Glenn, 2008), tree mortality estimates (Dalagnol et al., 2021), and estimation of the carbon saturation (Detto et al., 2015). As well, this data is also used for archaeology (Maté-González et al., 2019), urban flood risk modeling (Noh et al., 2018; Almeida et al., 2018), mapping power transmission lines (Yan et al., 2014; Dong & Chen, 2018; Chen et al., 2022a), road extraction (Chen et al., 2022b; Wang et al., 2022), urban change detection (Aljumaily et al., 2021; Zováthi et al., 2022), natural hazards (Trepekli et al., 2022) and many others.

METHODOLOGY

Location and description of the study area

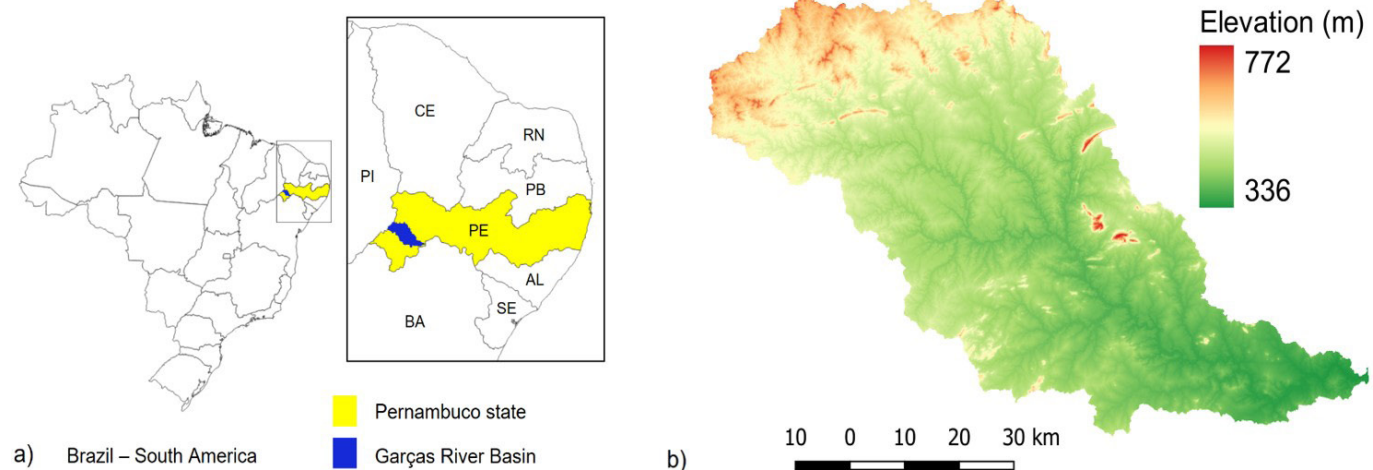


Figure 1. (a) Location of the study area in Brazil and within Pernambuco state; (b) Digital Terrain Model of Garças River Basin from LiDAR survey.

The Garças River basin (Figure 1), located in the region called Sertão, west of the State of Pernambuco, is taken as a study case. The major river of this basin has its headwaters on the border of Pernambuco with Piauí, being initially called Caipora stream, and continues until the São Francisco River, where it ends. Its total length is approximately 192 km, draining an area of 4,094.10 km², which represents 4.16% of the state's area and is fully inserted in it. It has eight large reservoirs, with a maximum storage capacity of over 1 million m³ (Agência Pernambucana de Águas e Clima, 2013).

The Garças River basin has an annual rainfall climatology varying from approximately 700 mm in the headwaters located on the northwestern part of the basin up to 400 mm in the southeastern region, near the basin outlet, according to the rainfall climatology map presented at Agência Pernambucana de Águas e Clima (2022). This basin also has a hot and dry climate and poorly distributed rainfall during the year. The relief is formed by vast flattened surfaces, presenting higher elevations to the north, in Araripe Highland. Land use in this basin is predominantly of open shrub vegetation, characteristic of the Caatinga, and anthropized regions, where areas of polyculture and pasture are interspersed with a few fragments of open tree shrub vegetation (Agência Pernambucana de Águas e Clima, 2013).

Data acquisition and preparing

The State of Pernambuco carried out an aerophotogrammetric survey with LiDAR, which began in 2014, covering the entire state (Cirilo & Alves, 2014; Cirilo et al., 2015). This program, called Pernambuco Tridimensional (PE3D), with the purpose to acquire high-resolution DSM and DTM, derived from LiDAR, in addition to orthoimages, both on two scales, 1:5,000 (for the entire territory) and 1:1,000 (for the main municipal headquarters). These scales correspond to a spatial resolution of 50 cm and 12 cm for the orthophotos; and of 1 m and 50 cm for the LiDAR data, respectively. The altimetric error of the laser tillering is better than 25 cm for the 1:5,000 scale, and better than 10 cm for the

1:1,000 scale (Cirilo & Alves, 2014; Cirilo et al., 2015; Amaral et al., 2020). All products presented are referenced in the Projected Coordinate System UTM SIRGAS 2000, in spindles 24S or 25S (Cirilo et al., 2015).

The State of Pernambuco has 98,146 km² of area, which was divided into 12,962 articulated scenes for the organization of the LiDAR data, with a cloud of 75 billion points (an approximate density of 1.3 per m²; Cirilo et al., 2015). In the Geotiff format of this data, each file has an average size of 39.5 MB, containing approximately 3,500 columns and 2,400 rows. The storage size needed for the entire original DTMLiDAR dataset in this format is approximately 512 Gigabytes.

Both DTM and DSM LiDAR data acquired for the study area present about 10.6 billion pixels each after concatenating the 739 scenes. Pixels with missing data were filled by a filtering approach, considering the average of neighboring pixels in a window of $n \times n$. The size of n is initially set to 3 for each pixel with missing data, but it is progressively enlarged if the number of valid pixels inside it is smaller than n .

The LiDAR DTM was further aggregated by the averaging method to produce coarser spatial resolutions DTM (2, 5, 10, and 30 m) and investigate the effect of spatial resolution change on both the computational cost and the river drainage network quality. Considering the number of individual scenes and the total amount of data and the operations involved (concatenate, filter, resample), a python programming routine was developed for automatically performing these procedures for the whole data set, avoiding the excessive, repetitive and time-consuming manual tasks.

The SRTM DEM with a spatial resolution of 30 m for the study area was also obtained from USGS. This data was also processed and used for comparing and analyzing topography and river drainage network quality relatively to the LiDAR DTM results, as the SRTM is the most widely used source of DEM (Schumann & Bates, 2018).

Topographic characterization

The topography of the study area is analyzed based on hypsometric curves and profile transects considering the three different data sources: LiDAR DTM (original and pixel aggregated), LiDAR DSM, and SRTM DEM. Both LiDAR and SRTM data used in this study have the geoid EGM96 as a vertical datum. In addition, a direct comparison between these raster files is performed by overlying them and relating the differences to distinct land use and vegetation cover, identified based on the orthophotos. For overlying LiDAR and SRTM data, the SRTM DEM is resampled to 1m spatial resolution by just dividing each 30-m pixel into 30x30 finer pixels of 1m with the same attribute of the coarser pixel.

Derivation and characterization of river drainage networks

For deriving river drainage networks from the DTM or DSM, three major steps were adopted: depression removal, flow direction determination, and flow accumulation. The former

is needed due to the occurrence of flat areas and depressions (one or more pixels surrounded by pixels with higher elevation). The depressionless DTM or DEM is then processed for determining the flow direction for each pixel. The last step is the determination of the upstream contributing area for each pixel, which is named the flow accumulated matrix.

Distinct algorithms for each of these 3 steps were used, to compare their relative computational efficiencies. The software TerrSET, RichDEM, and SAGA GIS were selected, because of the following reasons: i) TerrSET is commercial and traditionally adopted by water resources researchers, with remarkable results regarding the quality of derived river drainage networks (e.g. Buarque et al., 2009; Siqueira et al., 2016); ii) RichDEM and SAGA GIS are freely available and present new algorithms proposed for dealing with large data sets and with outstanding efficiency results reported (Wang & Liu, 2006; Barnes, 2018).

Depressions removal

Four algorithms of depressions removal were tested: Pit Removal TerrSET (Sedgewick, 1992), Depression-Filling RichDEM (Barnes, 2016), Fill Sinks SAGA GIS (Wang & Liu, 2006), and Fill Sinks XXL (Wang & Liu, 2006). The Pit Removal algorithm creates an adjusted DEM by breaching depressions, or local minima. From the lowest altitude pixel of the analyzed depression, a path that directs the flow out of this depression is searched. The starting cell is the pit cell, and the ending cell is the cell that has a lower value than the pit along the flow path, or it is the cell located at the edge of the data set. Then, the pixels on that path are linearly lowered according to the distance covered (Sedgewick, 1992). The resulting raster ensures that any cell in the image can follow along a path to its edge. A path is composed of cells that are adjacent horizontally, vertically, or diagonally in the raster grid and decrease steadily in value. The Pit Removal TerrSET algorithm is computationally limited to raster matrixes smaller than 32,000 rows and columns (TerrSET Manual).

The depression filling algorithm provided by RichDEM simulates an artificial flood of the DEM from the edge into the raster, using a priority queue to determine the next cell to be flooded. Edge pixels are marked as resolved as they ensure they drain away from the raster. The processing takes place through the insertion of border pixels in the priority queue, the one with the highest priority will always be the one with the lowest altitude. The highest priority pixel is removed from the queue and its neighboring pixel is analyzed. If the neighboring pixel under analysis has a higher altitude than the removed pixel, it is added to the priority queue and processing continues unchanged. Otherwise, it is inserted into a simple queue and its altitude value is replaced by the same pixel value that was removed from the priority queue. The next iteration again analyzes the neighbor of the lower pixel, now analyzing both queues. Processing ends when there are no more pixels in the priority queue. To overcome the RAM limit to deal with the entire data set, this algorithm divides the DTM into tiles if necessary. This algorithm is capable of processing large amounts of data even on personal computers, but its performance is favored if it is processed in more robust computational environments (Barnes, 2016). Access to physical

and volatile memory is reduced by this algorithm, as a way to reduce resources and reduce computational cost – for instance, processing two trillion pixels in 287 min (Barnes, 2016).

The SAGA GIS Fill Sinks algorithm also uses the filling idea to remove sinks. In addition, this method proposes the removal of depressions by changing the original DEM as little as possible, and even so, it guarantees a downward slope along the flow path. This algorithm prioritizes the lowest cost search for optimal flow paths and it uses the concept of spill elevation, assigning to the entire study area a water mirror of higher altitude and decreasing it until it finds all the drainage points (Wang & Liu, 2006). Another version of this algorithm is specifically designed for processing large data sets, particularly LiDAR data, and is named Fill Sinks XXL.

Flow direction determination

The D8 flow direction method (Deterministic eight neighbors; Marks et al., 1984; O’Callaghan & Mark, 1984; Jenson & Domingue, 1988) identify and assign to each pixel a unique flow direction towards the greatest slope between the central pixel and its neighbors. To calculate the slope, the elevation values and the distance between them are used, with the distance between orthogonal pixels being equal to the spatial resolution ($dx = \text{spatial resolution}$); and between diagonal pixels equal to the product of the square root of two by the spatial resolution ($dx = \sqrt{2} \times \text{spatial resolution}$). For all three software used in this research, the approach of considering a single flow direction for each pixel was adopted, based on the D8 method.

Flow accumulation calculation

For a given pixel, the accumulated flow is the sum of all pixels draining to this pixel. This information can be expressed as the number of upstream pixels contributing to this pixel or considering the sum of their surface areas. This is a simple concept, but distinct software may adopt specific computational methods to achieve this calculation, mostly trying to reduce the run time. The computational cost of calculating the accumulated drainage areas of refined spatial resolution DEMs using conventional methods can be prohibitively long. For this reason, in recent years, new algorithms have been proposed to reduce computational costs and enable the use of these data for large areas (pa; Zhou et al., 2019).

The following algorithms were used: RUNOFF TerrSET algorithm; RichDEM Flow Accumulation algorithm; SAGA GIS D8 Flow Accumulation (Top-Down) algorithm. The RUNOFF TerrSET algorithm is based on the former method proposed by Jenson & Domingue (1988). This algorithm calculates the flow accumulation of each pixel from the MDE raster based on the concept of a unit of rainfall “dropped” on every pixel flowing along its downstream flow path until it reaches the boundary of the data set. The RUNOFF TerrSET algorithm is computationally intensive and cannot run on large images (TerrSET Manual). The tool Flow Accumulation (Top-Down) of SAGA GIS software processes a DEM downwards from the highest to the lowest cell and can process large data sets.

The RichDEM Flow Accumulation algorithm uses distributed processing. It uses a segmentation approach to divide and process the study area into partitions, master and slave nodes, with only two communication between the master and each slave node (Barnes et al., 2016). This bounds the communication, reduce the processing time and allow the algorithm to be processed for large DEM on conventional desktops (Barnes et al., 2016).

Evaluation of river drainage networks quality

In this step, just the river drainage network derived by the algorithms present in SAGA GIS was evaluated, aiming at comparing the results from using SRTM DEM and LiDAR DTM with different spatial resolutions. It was beyond the scope of this paper to make comparisons among the distinct algorithms of DEM processing.

Firstly, the derived networks were visually compared to a vector river network manually digitized over orthophotos for some reaches of the main river of the basin. This visual comparison approach has been widely used in literature (e.g. Moretti & Orlandini, 2018; Ariza-Villaverde et al., 2015; Nikolakopoulos et al., 2015; Persendt & Gomez, 2016; Woodrow et al., 2016; Lai et al., 2016; Lindsay, 2016), considering the human eye and brain ability to easily analyze patterns typically found in river drainage structures (Arora & Harrison, 2007; Saraiva & Paz, 2014), despite its inherent subjectivity and risk of bias (Saraiva & Paz, 2014; Sousa & Paz, 2017).

The second approach was the analysis of river characteristics such as length, sinuosity, and slope, and basin characteristics such as drainage area and drainage density. Despite minimizing the spatial component of the comparison (Gatziolis & Fried, 2004) and presenting the error compensation effect (Sousa & Paz, 2017), this analysis is relevant as these river characteristics are useful for several environmental and hydrological studies. The third analysis was the direct comparison between basin delimitations, computing commission, and omission errors. For the second and third analyses, the results obtained for the LiDAR 1 m-DTM were considered as the reference for evaluating the results from the coarser LiDAR DTMs and the SRTM DEM, as no independent and reliable source of information was available.

Computational resources and computational cost

The computational cost was quantified in two ways. The first one refers to the disk space requirement for storing each DTM/DEM for the whole Garças river basin and its derived main products related to the steps for obtaining the river drainage networks: depression removal, flow directions determination, flow accumulation calculation, basin delimitation, and river drainage network extraction. Each of these steps produces a raster matrix with the same number of rows and columns of the input DTM/DEM, but varying the data format: the input DTM/DEM, the depressionless DTM/DEM, and the flow accumulation matrix were considered as float; the rasters of flow directions, basin limitation and river drainage network were considered as integer format.

The second aspect of the computational cost quantification was the computational time, defined here as the length of time required to separately and completely perform two operations: depression removal and flow accumulation calculation for the whole Garças river basin. These procedures are the most time-consuming steps for deriving a river drainage network from a given DTM/DEM. Each time one of these operations was carried out the computer was fully dedicated to this aim, not using it for any other user demand, as well as turning off software updating, antivirus scanning, background software, and operational system hibernating and sleeping, and computer restarting for cleaning RAM cache. Additionally, each of these operations for a given DTM/DEM was performed twice, to guarantee that non-predicted, isolated events could have influenced the computational run time.

Two configurations of computational resources were adopted to analyze the efficiency of the algorithms for DEM/DTM processing (Table 1). The first one is a desktop with a processor, system RAM, and graphics very common to current low-cost computers, which represent computational resources typically available for most users – referred to as desktop. The second one is a workstation with a processor, system RAM, and graphics of higher capacity than the first. The workstation's great difference is that in addition to having 4 times the amount of RAM as the desktop, its RAM also has an ECC (Error Correction Code), capable of correcting data reading and writing bugs, during processing, avoiding possible system crashes.

Summary of evaluation procedures

A summary of all the analyses performed in this research is presented in Table 2, specifying which topographic data source and spatial resolution are considered in each case. The analysis of topography encompasses three approaches. First, the calculation

of the DEM of differences and the elaboration of topographic profiles make a comparative analysis between SRTM DEM, LiDAR DTM 1m, and LiDAR DSM 1m, considering Orthophoto images as auxiliary data to aid in interpreting the results. Further, the determination of hypsometric curves compares the LiDAR DTM coarsening relatively to its finer resolution, as well as relatively to SRTM DEM.

The effect of different topographic data sources and spatial resolution on river drainage network quality is evaluated by visual inspection regarding its ability to follow the drainage patterns identified on the Orthophotos. The derived river networks are also quantitatively evaluated by comparing the main river reach length, sinuosity, and slope, as well as by comparing basin drainage area, drainage density, and basin delineation.

Finally, the computational cost for working with LiDAR DTM in different spatial resolutions is assessed regarding two issues: i) disk space requirements for storing DEM data and derived products; ii) runtime for depressions removal and flow accumulation, considering distinct algorithms.

RESULTS AND DISCUSSION

Topographic analysis

In general, it can be observed that the DTM topographic profiles characterize the bare earth surface, i.e. without human-made materials and natural elements on it, while the DSM profiles present both the bare surface and the natural and artificial elements on it (Figure 2). For instance, in the topographic transect A-G crossing an urban area (Figure 2a), there is a huge shed almost 10 m high (point B) which is represented in the DSM but not in the DTM, as well as other buildings and houses near point

Table 1. Computational infrastructures used for DEM/DTM data processing.

	Processor	System RAM	Data bus	Graphics
Workstation	Intel Xeon E5-2666 v3 3.5 GHz	64 GB ECC	64 bits	Dedicated - NVIDIA® GeForce 8400 GS 256 MB
Desktop	Intel Core i5-8,400 2.80Ghz	16 GB	64 bits	Integrated - Intel UHD 630

Table 2. Evaluation procedures and corresponding topographic data source, spatial resolution, and auxiliary data.

Analysis	SRTM DEM 30m	LiDAR DSM 1m	LiDAR DTM 1m	LiDAR DTM 2m, 5m, 10m, 30m	Auxiliary data
DEM of Differences	yes	yes	yes	-	Orthophotos
Topographic profile	yes	yes	yes	-	Orthophotos
Hypsometric curves	yes	-	yes	yes	-
Visual inspection of river drainage networks	yes	-	yes	yes	Orthophotos
Main river reach length, sinuosity, and slope	yes	-	yes	yes	-
Basin drainage area and drainage density	yes	-	yes	yes	-
Basin delineation	yes	-	yes	yes	-
Computational cost – disk space to store DEM and derived products related to drainage network extraction	yes	-	yes	yes	-
Computational cost – runtime for depressions removal with distinct algorithms	-	-	yes	yes	-
Computational cost – runtime for flow accumulation with distinct algorithms	-	-	yes	yes	-

D. Areas of the bare surface make DSM and DTM be the same (point E, for example).

Areas of dense vegetation cover highlight larger differences between DSM and DTM, of up to 10 m, like the region around point J in Figure 2b. Interestingly, the sharp transition from forest to open field is very marked (point K). Near point F in Figure 2a the transect crosses a large paved road. Road embankments may be considered continuity of the bare surface and thus it remains represented in the LiDAR DTM, unlikely to bridges, that were explicitly removed when producing the DTM from the PE3D data (Instituto de Tecnologia de Pernambuco, 2018a, 2018b).

Despite the LiDAR PE3D survey not being capable of penetrating the water, the river cross-section near point C is satisfactorily represented in both DTM and DSM, probably due

to the very reduced water level at the time of the survey. As this is a narrow river and due to inherent uncertainties and inaccuracy of SRTM DEM relatively to this level of detail, there is not an explicit representation of this river cross-section on this data.

In wider regions without vegetation cover (like point E in Figure 2a), there is more agreement between SRTM and LiDAR data. However, the difference of almost 15 years in the period of data acquisition between the SRTM and PE3D surveys hinders more conclusive comparisons. For instance, deforested areas like nearby points I and L could be covered by dense vegetation during SRTM data acquisition. During this 15-year time-lapse, changes may also have occurred on the topographic profile due to population dynamics and interventions, and nature itself. Furthermore, any analysis of SRTM data should not disregard its coarse spatial resolution (30 m), and its absolute and relative elevation errors of 16 and 6 m, respectively (Rabus et al., 2003, Farr et al., 2007; Hawker et al., 2018; Schumann & Bates, 2018), and the known vegetation effect (O’Loughlin et al., 2016; Grohmann, 2018; Yamazaki et al., 2019).

The DEM of differences (DoD) between SRTM DEM and LiDAR DTM shown in Figure 3 presents values ranging from -22 m up to +39 m. There is a large predominance of positive differences (86% of the area), with 65% between 0 and 4 m, and only 1.3% larger than 8 m. This DoD is coherent to the vertical precision of the SRTM and the predominance of medium-sized vegetation and small buildings and emphasizes the DSM nature-like of the SRTM DEM. Also, this figure shows the DoD between LiDAR DSM and LiDAR DTM for the same area. The differences are in general closer to zero than in the previous DoD, with 79% of them positive: 75% between 0 and 4 m, 3% between 4 and 8m, and only 1% larger than 8 m. These positive differences are by the predominance of bare earth surface with sparse vegetation and minor occurrence of small buildings. The negative differences (21% of the area) are largely very small (99% of them are less than 1 m; 81% of them are less than 0.2 m), and may be related to the maximum altimetric error of 25 cm reported by (Instituto de Tecnologia de Pernambuco, 2018a, 2018b), inherent inaccuracies

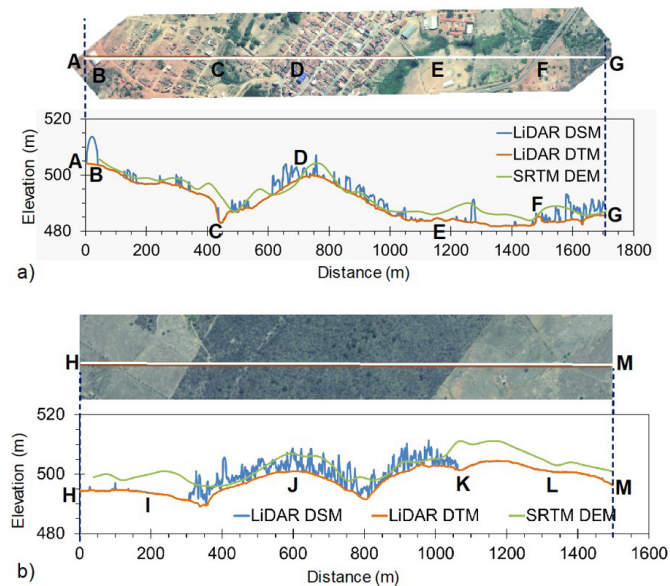


Figure 2. Topographic profiles along two transects over the study area, considering elevation from LiDAR DSM, LiDAR DTM, and SRTM DEM.

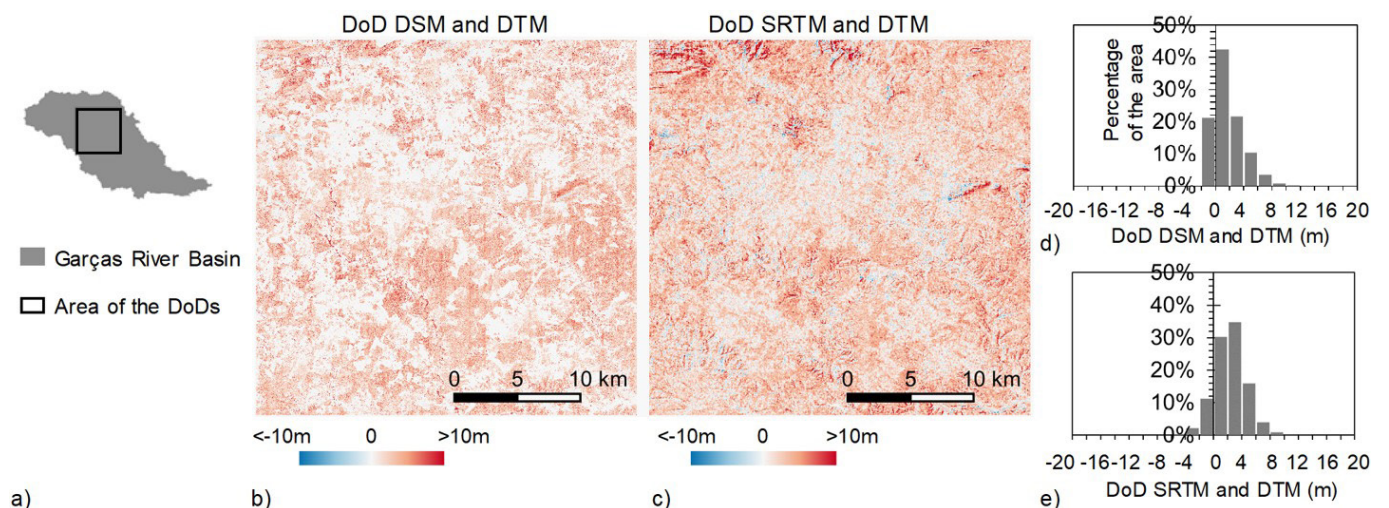


Figure 3. (a) Area selected for analyzing the DEM of differences (DoD) between LiDAR DSM 1m and LiDAR DTM 1m (b), and between SRTM DEM and LiDAR DTM 1m (c); (d), (e) Frequency histograms of the DoDs.

of data treatment for obtaining both DSM and DTM and different noise effects.

For another region, located in the south-eastern part of the Garças river basin and that is part of the Santa Maria municipality, Figure 4a highlights the marked effect of buildings on elevations represented in the DSM and that was removed in the DTM representation of the bare earth. On the contrary, the SRTM DEM does not present a spatial distribution of elevations that resembles the spatial location of buildings, mostly due to its coarse resolution relative to the buildings' sizes. Another remarkable example of differences between DSM and DTM is the bridge removal of the federal road BR-122 in the central portion of the basin (Figure 4b). The DTM is approximately 13 m lower than the DSM in the location of this bridge. In the vicinity of the same area, riparian forest trees higher than 10 m were also removed.

The differences between SRTM DEM and LiDAR DTM are dampened when the purpose is the construction of the hypsometric curve of the basin (Figure 5a). In the mentioned figure, the blue lines and the light green line do not appear due to be practically the same as the dark green one, which is positioned on the top of them. There are numeric differences of less than 2.3% between corresponding points of these hypsometric curves (Figure 5b). For instance, 50% of the basin is higher than an elevation of 460 m according to SRTM DEM data, while this elevation is about 458 m according to the LiDAR DTM. A hypsometric curve represents the global topographic distribution of a basin relief and may be influenced by a sort of compensation effect between areas of

under- and overestimation of elevations when comparing two topographic data sources.

Evaluation of derived drainage networks

Rivers flowing in the Garças river basin are relatively narrow, with the main channel of few meters wide, and most of them are intermittent, as this is a semi-arid area. These characteristics make these rivers difficult to be adequately represented in DTM-derived networks and to be visually identified on the orthophotos.

An example of the visual inspection for quality evaluation of the derived river networks is shown in Figure 6. Part a of this figure highlights the agreement between the LiDAR DTM 1m – derived river drainage network and the actual river pathways seen on the underlying orthophoto. In this figure, three detailed zooms illustrate that the DTM-extracted river network fits entirely in the main channel visually perceived in the orthophoto for some river reaches, while for other reaches there is a displacement of a few meters wide. For instance, this displacement is up to 8 meters in the zoom shown in the central part of the mentioned figure.

Coarsening the DTM resulted in derived drainage networks that maintained very satisfactorily the spatial patterns shown in the finest resolution. For the example shown in Figure 6, the differences between the 1 m- and 2 m-derived networks are almost visually imperceptible. The 5 m- and 10 m-extracted networks also present minor and punctual differences to the finest resolution. The coarsest resolution (30 m) still conserves most of the river

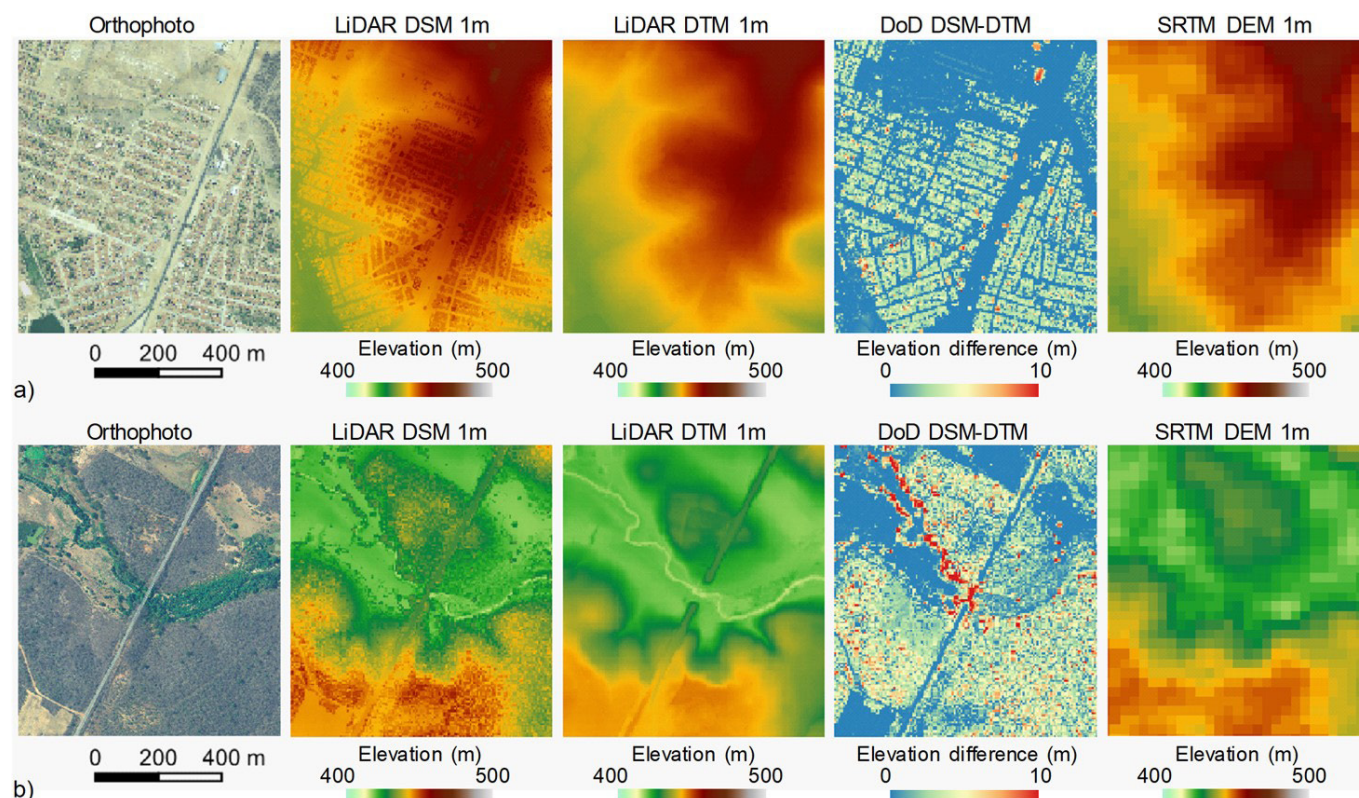


Figure 4. (a) Example of buildings removal from the DSM to the DTM on LiDAR data for part of the Santa Maria municipality in the south-eastern region of the Garças river basin; (b) Example of a bridge and tree removal from the DSM to the DTM.

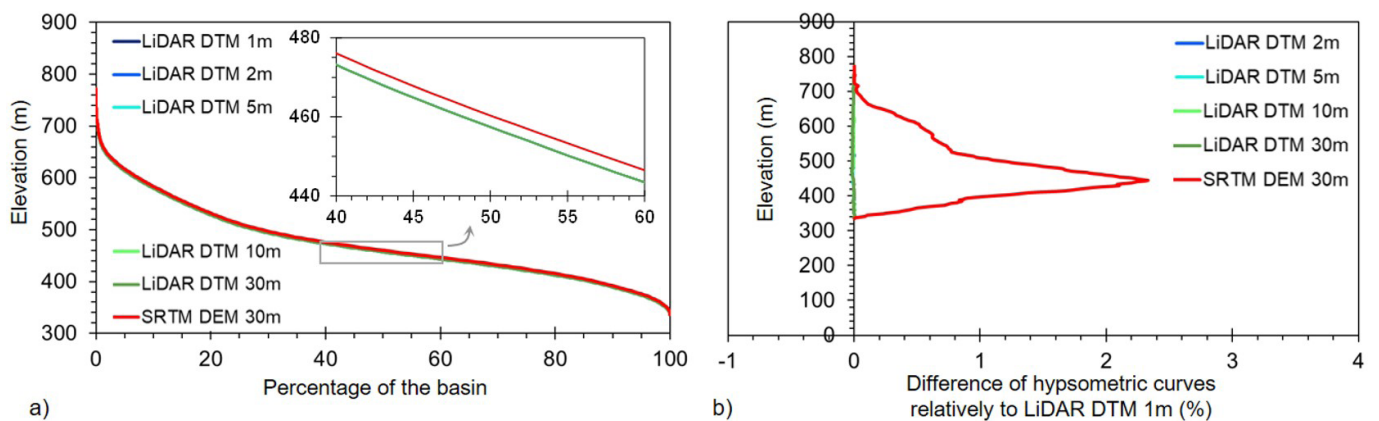


Figure 5. (a) Hypsometric curves of Garças river basin derived from the LiDAR DTM of different spatial resolutions and the SRTM DEM; (b) Differences of hypsometric curves relative to the one derived from the LiDAR DTM 1m.

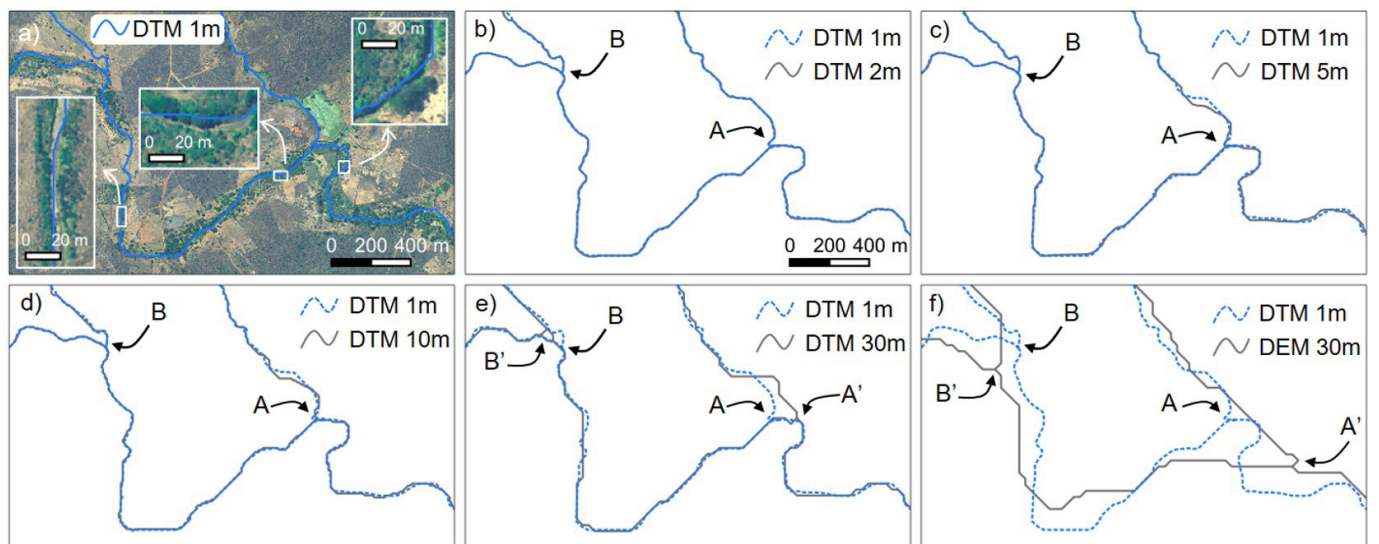


Figure 6. (a) Orthophoto and LiDAR DTM 1m-extracted river network; (b), (c), (d), (e) Overlay between river drainage networks derived from resampled LiDAR DTM and the finest resolution DTM; (f) Overlay between river drainage derived from SRTM DEM 30m network and LiDAR DTM 1m-derived network.

paths quite similar to the 1 m-network, but there are noticeable divergences between them in some river reaches. For example, river junctions A and B of the 1 m-network are offset by nearly 100 m in the 30m-network (points A' and B').

However, the quality of the LiDAR 30 m network is better than the SRTM 30 m network. The latter presents a considerable displacement from the 1m-network along its entire length – for instance, river junctions A and B are now offset by roughly 180 m and 370 m, respectively. There is also a general tendency of smoothing the meanders of the river flow paths in the SRTM network, as can be seen on both river reaches upstream of junction A' relatively to their counterparts upstream of junction A in the 1m-network. This effect is due to the coarse size of the SRTM pixel relative to the dimensions of the actual river meanders in the area, an effect widely reported by other authors (Fekete et al., 2001; Yang et al., 2014).

The high quality of the LiDAR DTM 1 m-derived network is a direct result of so refined topographic representation achieved

by this 1 m-DTM. Nevertheless, this ability of the 1 m-DTM for representing small-scale variations of the topography also presented some pitfalls when deriving the river drainage network. A clear example of this is the case of an intermittent river reach in which the wider main channel is dry and there are two narrow, parallel courses represented in the topography (Figure 7a), separated one from another by a distance varying between 80 m and 160 m. The 1 m-DTM was able to accurately represent these topographic characteristics (Figure 7b), while the SRTM DEM is too coarse to capture these details, and roughly represents the wider channel (Figure 7c).

As a consequence, the DTM 1m-derived network has two parallel flow paths (pointed by arrows A and B in Figure 7d) representing this river reach. This is reasonably correct regarding the actual topography, but may be considered a misrepresentation of the river network. During higher water levels, the water occupies the wider channel embracing together both A and B flow paths. Thus the tributary in the upper right part of the figure should

confluence to the main river flowing from the left part near point C in Figure 7b. Instead, due to the division of the main river course into two distinct, parallel flow paths, the confluence C occurs far downstream (point C' in Figure 7d), approximately 1.8 km in a straight line and 2.2 km along the main river course. The use of the river network with these A and B parallel flow paths would not be adequate as input data for running a hydrological model to predict floods in this area, for example.

Consider now the use of the river drainage network in Figure 7d for basin delineation. If the basin outlet is selected along the parallel flow paths A or B, the result would be quite distinct and considered wrong. An outlet located on flow path A would result in a basin restricted to the area contributing to this river reach, disregarding the areas draining to flow path B, and vice-versa. The expected basin delimitation should instead comprise drainage areas of both the main river course and its tributary. So, these parallel flow paths are not desired to be present for purposes of most hydrological studies.

The drainage networks derived from coarse DTMs of 2 m (not shown), 5 m (not shown), and 10 m (Figure 7e) present the same parallel flow paths pattern observed for the 1 m. The 30 m

resolution was so coarse that this parallelism was avoided (Figure 7f), just as it occurred in the SRTM-derived network (Figure 7g). However, the confluence D that is reasonably represented in the finer DTM-derived networks (Figures 7a and 7b) and also in the DTM-30 m network, is displaced by 330 m in the SRTM network.

Analysis of river and basin characteristics

The effect of LiDAR DTM coarsening on basin and river drainage characteristics is illustrated by the results shown in Figure 8. Overall, as depicted by the visual inspection analysis, enlarging the pixel size of the DTM led to shortening the river flow paths. This effect is negligible for the 2 m and 5 m spatial resolutions, which resulted in a reduction of river lengths by 0.1 and 0.3%, and is slightly present on 10 m resolution (main river length reduction of 1.2%). The LiDAR coarsest resolution still achieved a reasonable result of just reducing by 4% the main river length, while the reduction was about 12% when the river length was derived from SRTM DEM. This result strengthens the

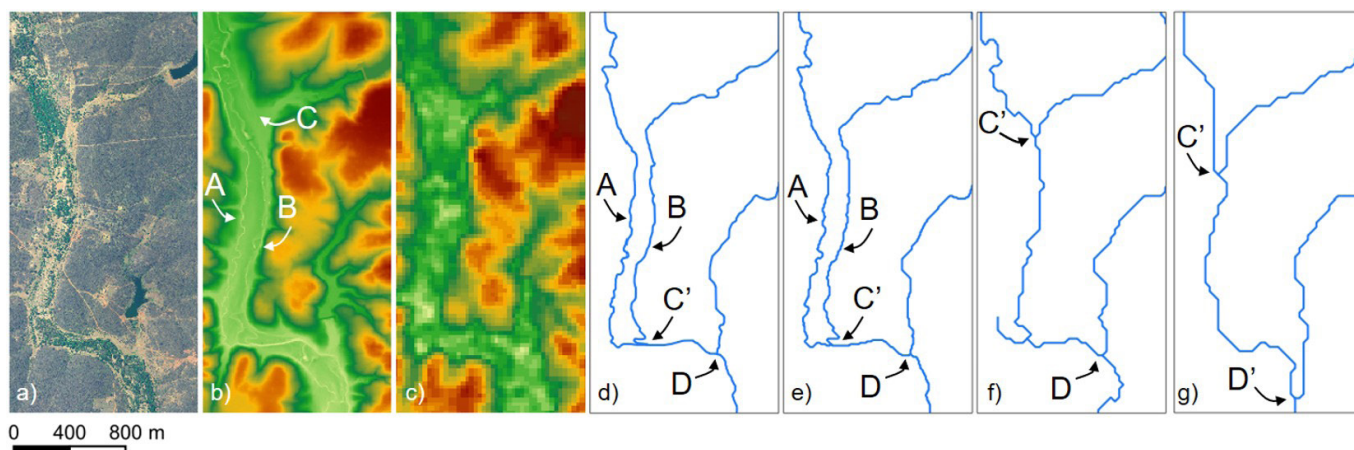


Figure 7. Example of main channel of an intermittent river reach with two parallel flow paths: (a) Orthophoto; (b) LiDAR DTM 1 m; (c) SRTM DEM 30 m; (d), (e), (f) LiDAR DTM 1m-, 10m-, and 30m-derived networks, respectively; (g) SRTM DEM 30m-network.

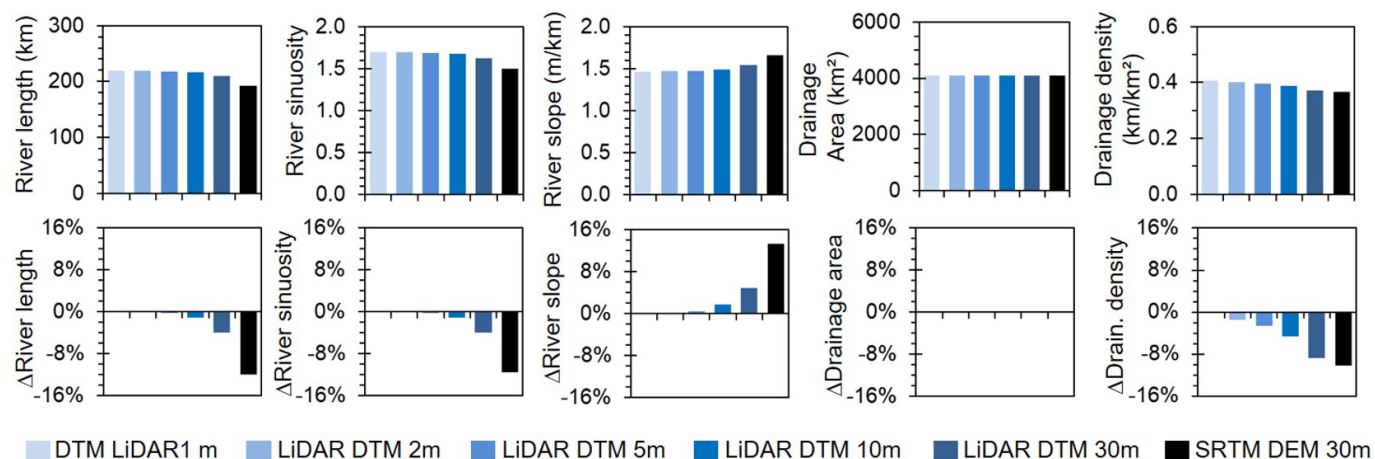


Figure 8. Garças river basin and river drainage characteristics derived from distinct LiDAR DTM and SRTM DEM, and percentage differences (Δ) relative to the LiDAR DTM 1m.

lower quality of the river flow paths obtained from SRTM relative to the LiDAR data in the same spatial resolution.

The same effect on river lengths is observed in river sinuosity, as shortening the river flow paths reduces proportionally the river sinuosity. The reduction of river lengths according to pixel size and topographic data source has also strongly influenced the comparative analysis of main river longitudinal slopes but oppositely. The lesser the river length the larger the slope. In comparison to the main river length variation, the slope variation was amplified because it combines the effect of main river length variation with the overall tendency of topographic smoothing according to pixel size coarsening. Again, negligible effect on river slope is observed for the 2 m and 5 m resolutions, while this effect is minor for the 10 m (1.8%), and reaches almost 5% for the 30 m-resolution. The SRTM-derived main river resulted in a 13.4% larger slope than the LiDAR DTM 1 m-network.

In contrast, the drainage area quantification was the same ($\sim 4100 \text{ km}^2$), regardless of spatial resolution and topographic data source. Even spatially comparing the basin delimitations there are tiny differences (omission and commission ‘errors’ less than 0.4%) among the results obtained for the distinct DTM and DEM relative to the 1 m-delineation (Figure 9). Combining this lack of variation of basin drainage areas with the effect of river length reduction according to pixel size coarsening explains the tendency of drainage density reduction. The largest reductions were obtained for the LiDAR DTM 30 m (8.9%) and SRTM DEM (10.3%).

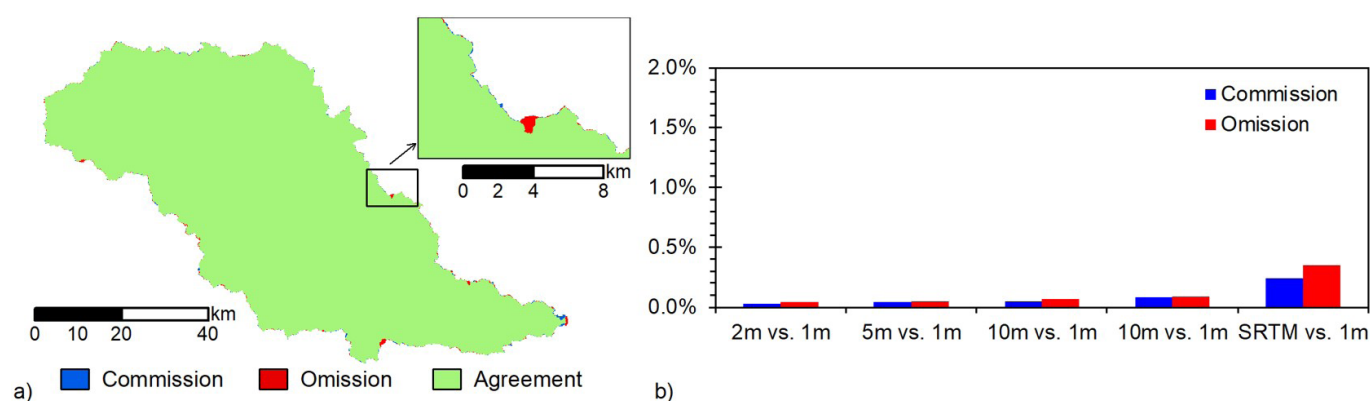


Figure 9. (a) Spatial comparison between Garças river basin delineation derived from SRTM DEM 30 m and LiDAR DTM 1 m, considering the latter as the reference; (b) Quantification of commission and omission areas in basin delineation for different LiDAR DTM spatial resolutions and SRTM DEM relatively to the LiDAR DTM 1m delineation taken as reference.

Table 3. Dimensions of the numerical matrix and corresponding data storage requirements for each LiDAR DTM and SRTM DEM of the study area, including derived products (rasters of depressionless DTM/DEM, flow directions, flow accumulation, basin delimitation, and river drainage network).

DTM/DEM Spatial resolution	Number of columns	Number of rows	Number of valid pixels (billions)	Size of the DTM/DEM (Gb)	Size reduction relative to 1m
DTM 1 m	127,556	82,992	5.706	39.439	-
DTM 2 m	63,778	41,496	1.426	9.860	-75.0%
DTM 5 m	25,511	16,598	0.228	1.578	-96.0%
DTM 10 m	12,755	8,299	0.057	0.394	-99.0%
DTM 30 m	4,251	2,766	0.006	0.044	-99.9%
DEM 30 m	4,390	2,640	0.012	0.043	-99.9%

Analysis of the computational cost of DTM/DEM processing

For the 1m-spatial resolution, the DTM of the Garças river basin has 127,556 columns and 82,992 rows, with 5.7 billion pixels with valid information to store and process (Table 3). This DTM requires disk space of 39.4 Gb and together with its derived products related to extracting river drainage networks the disk space used reaches 177.5 Gb (Figure 10a). For the sake of comparison, the representation of the whole Amazon basin ($5,084,460 \text{ km}^2$ according to Lakshmi et al., 2018) within SRTM DEM 30 m data comprises nearly 5.6 billion pixels. Thus storing and processing LiDAR DTM with 1 m spatial resolution for the Garças river basin (“only” $4,100 \text{ km}^2$) is comparable to storing and processing SRTM DEM 30 m to the world’s largest basin, and far harder than working with SRTM DEM 30 m to represent the second world largest basin (Congo river basin, with $3,064,930 \text{ km}^2$; Lakshmi et al., 2018).

A proportional analysis indicates a required disk space of 43.4 Gb for each $1,000 \text{ km}^2$ of DTM and derived products with 1 m spatial resolution. For the Garças river basin, DTM coarsening to 2 m spatial resolution reduced by 75% the size of the matrix and the corresponding disk space requirements relative to the 1 m-resolution. This reduction achieves 96% when the pixel size is enlarged to 5 m and reaches 99% and 99.9% for the 10 m- and 30-m resolutions, respectively.

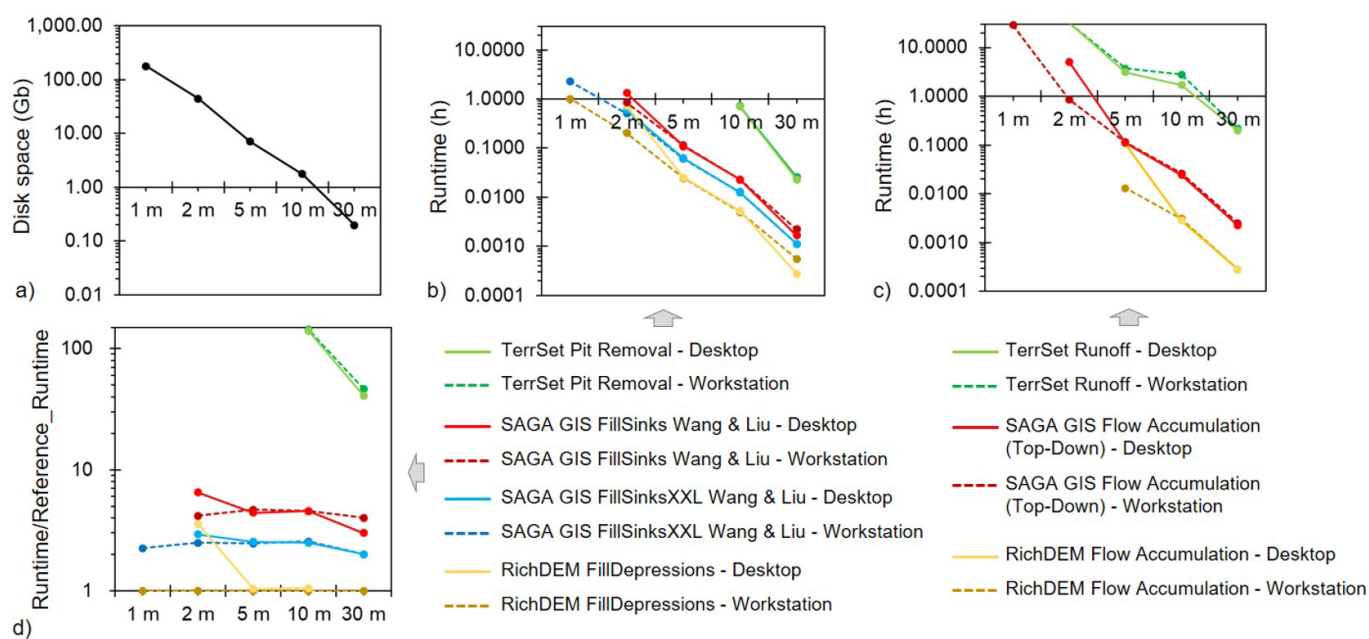


Figure 10. (a) Disk space needed to store DTM and derived products related to drainage network extraction for the Garças river basin considering different spatial resolutions; (b) Computational runtime for DTM depression removal using distinct algorithms and computers; (c) Computational runtime for flow accumulation using distinct algorithms and computers; (d) Runtime for DTM depression removal for each algorithm and computer divided by the runtime achieved by the RichDEM FillDepressions Algorithm running in the Workstation, considered as the reference here.

Accordingly, the large differences in the number of pixels to process following DTM coarsening also resulted in very distinct computational runtimes for depression removal and flow accumulation (Figure 10b and Figure 10c), independent of the algorithm and computer. Refined spatial resolutions, as expected, demand more processing time and a robust computational infrastructure to process them. For a given spatial resolution, the results were distinct among the algorithms and between the two computers. However, the coarser the spatial resolution, the smaller the runtime differences among algorithms and computers. In other words, for larger datasets, there is more relevance in selecting efficient algorithms and using a powerful computer.

For depressions removal, runtime ranged from a few seconds for the coarsest resolution to approximately 2h 16min for the finest resolution. The RichDEM FillDepressions algorithm was systematically the fastest one, while the TerrSet Pit Removal was markedly slower than the others (runtime roughly 100 times slower than RichDEM; Figure 10d). The SAGA GIS FillSinksXXL algorithm was 2-3 times slower than RichDEM, but proved to be more efficient than its similar SAGA GIS FillSinks algorithm (3-6 times slower than RichDEM).

However, some runs of all algorithms were not achieved due to memory requirements. The TerrSet algorithm was striking the most restricted, not running the three finest resolutions (1 m, 2 m, and 5 m) using both computers. The 1 m-spatial resolution has also hampered the calculus for the other algorithms: the SAGA GIS FillSinks algorithm did not run for the 1 m resolution on both computers, while the SAGA GIS FillSinks XXL and RichDEM algorithms did not run for the 1 m resolution in the Desktop machine. Thus, if only this low-cost, simpler computer

was available, the 1 m-spatial resolution depressionless DTM could not have been generated using any of the four algorithms tested in this research.

The removal of depressions in the TerrSet software has a limitation to processing data with more than 32,000 rows and columns, which is inherent to the algorithm and independent of the computer. In addition, it requires a large amount of RAM, which limits its applicability to LiDAR data. The use of RichDEM depends on libraries external to the solution, making its results linked to the ability of these libraries to handle raster files with a large number of rows and columns.

For the flow accumulation procedure, again the RichDEM algorithm was the fastest one, but it did not run for the 1 m- and 2 m-spatial resolutions due to an unclear error related to arrays dependence creation during algorithm execution. Several run trials were carried out, but the error remained. This result highlights the complexity required for using such an algorithm.

The TerrSet Runoff algorithm was again the slower one, with the additional issue that the depressionless DTM generated with the SAGA FillSinks XXL algorithm was used as input for the 1, 2, and 5 m resolutions, as the TerrSet Pit Removal algorithm did not run for these resolutions. Even so, the Runoff algorithm's runs for 1 m and 2 m resolutions were stopped after 33 h of calculation, to avoid a very long wait for results, considering that the computer had to be fully dedicated to this task during this period.

Just the SAGA GIS algorithm was able to process the flow accumulation procedure for the 1 m-spatial resolution, and this was accomplished only when using the Workstation (processing time 29h 4min). Thus, again the low-cost desktop machine was unable to perform this task regardless of the algorithm.

CONCLUSIONS

This paper evaluated the capabilities and shortcomings of using high-resolution LiDAR DTM for characterizing the topography and the river drainage, as well as comparing it relatively to using coarsened DTMs, and alternatively the SRTM DEM.

The computational cost for storing and processing the LiDAR DTM with 1 m spatial resolution for deriving river drainage networks may be quite prohibitive for most users, even when the study area is relatively small as a few thousand square kilometers. Specialized algorithms proposed in the literature and used in this research proved to be largely efficient for realizing these tasks, making them indispensable to deal with large data sets as so fine DTM. The algorithms proposed in the RichDEM software for depression removal and flow accumulation were the most efficient among the algorithms tested, followed by the algorithms available from the SAGA GIS software. However, still there are shortcomings in using these software and their algorithms.

Softwares like RichDEM do not present a user-friendly interface and request relatively strong expertise and effort of the user to configure the computational environment, install the required libraries, run the algorithms, and solve runtime errors. The latter has hindered the flow accumulation calculation for the finest resolution DTM using the RichDEM algorithm. These issues are not simple to solve and are a major drawback for the wider usage of these algorithms by most water resources researchers and professionals. The further evolution of this type of software should focus on making it easier to be applied, or implementing it as a subroutine of an already existent, well-known, and widely used software such as SAGA GIS. This software presents such a user-friendly interface and is ready to be applied without any complex knowledge by the users. However, its algorithm for flow accumulation is not efficient for handling large datasets.

Another shortcoming highlighted by this research was the large dependency of both depression removal and flow accumulation tasks on the system RAM, seriously limiting its applicability for large datasets with low-cost computers.

The terrain representation provided by the 1 m-LiDAR DTM is impressive, resulting in the overall outstanding quality of the derived river drainage networks. In occasional situations, the excessive information captured and represented in the 1 m-LiDAR DTM may lead to undesired patterns in river flow paths, as the representation of a reach of the main river channel by two river courses running in parallel.

The DTM coarsening to 2 m and 5 m spatial resolutions proved to be a viable alternative for maintaining a high-quality topography representation and preserving the derived river drainage networks with negligible discrepancies from the 1-m derived flow paths, while causing enormous reductions on both runtime and disk space requirements. Even the 10-m and the 30-m derived networks mostly resemble the finer 1-m network patterns and could be adopted for some studies with minor effects. The LiDAR 30-m networks showed to have much better quality in reproducing the expected river drainage flow paths than the SRTM DEM-derived network within the same spatial resolution.

In summary, the LiDAR topography survey provides data with outstanding quality, and this type of survey should be encouraged to be carried out for other parts of the Brazilian

territory, representing a new level of representing both terrains and derived river drainage networks. This type of data requires considerable adaptation of algorithms, methods, computational power and storage, and research. Working with spatial resolutions such as 5 m or 10 m is an alternative to achieving a better balance between data quality and computer requirements, according to the findings of this research.

ACKNOWLEDGEMENTS

The authors thank the Government of the State of Pernambuco for providing the PE3D data; the LACMA (Laboratório de Análises Computacionais em Meio Ambiente) from the Universidade Federal da Paraíba (UFPB) for the infrastructure; financial support from the CNPq (Conselho Nacional de Desenvolvimento Científico e Tecnológico) through Chamada Universal – MCTI/CNPq N° 01/2016 and research productivity grant for the second author; and CAPES (Coordenação de Aperfeiçoamento de Pessoal de Nível Superior) and FAPESQ (Fundação de Apoio à Pesquisa do Estado da Paraíba) for the scholarship for the first author.

REFERENCES

- Agência Pernambucana de Águas e Clima – APAC. (2013). *Relatório de situação de recursos hídricos do Estado de Pernambuco 2011/2012* (116 p.). Recife. Retrieved in 2022, November 14, from <https://www.lai.pe.gov.br/apac/wp-content/uploads/sites/9/2019/03/Relat%C3%B3rio-de-situa%C3%A7%C3%A3o-de-recursos-h%C3%ADricos-do-Estado-de-Pernambuco-APAC-2011-2012.pdf>
- Agência Pernambucana de Águas e Clima – APAC. (2022). *Sobre acumulado de chuvas*. Recife. Retrieved in 2022, November 14, from <https://www.apac.pe.gov.br/sobre-meteorologia/113-sobre-meteorologia/502-acumulado-de-precipitacao>
- Aljumaily, H., Laefer, D. F., Cuadra, D., & Velasco, M. (2021). Voxel change: big data-based change detection for aerial urban LiDAR of unequal densities. *Journal of Surveying Engineering*, 147(4), 04021023. [http://dx.doi.org/10.1061/\(ASCE\)SU.1943-5428.0000356](http://dx.doi.org/10.1061/(ASCE)SU.1943-5428.0000356).
- Almeida, G. A. M., Bates, P., & Ozdemir, H. (2018). Modelling urban floods at submetre resolution: challenges or opportunities for flood risk management? *Journal of Flood Risk Management*, 11, S855-S865. <http://dx.doi.org/10.1111/jfr3.12276>.
- Amaral, F. E., Cirilo, J. A., & Ribeiro Neto, A. (2020). Uso de técnicas de geoprocessamento na otimização do traçado de sistemas adutores de abastecimento de água com a utilização de uma base de dados de alta definição. *Engenharia Sanitária e Ambiental*, 25(2), 381-391. <http://dx.doi.org/10.1590/s1413-41522020193734>.
- Ariza-Villaverde, A. B., Jiménez-Hornero, F. J., & Gutiérrez de Ravé, E. (2015). Influence of DEM resolution on drainage network extraction: a multifractal analysis. *Geomorphology*, 241, 243-254. <http://dx.doi.org/10.1016/j.geomorph.2015.03.040>.

- Arora, V. K., & Harrison, S. (2007). Upscaling river networks for use in climate models. *Geophysical Research Letters*, *34*(21), L21407. <http://dx.doi.org/10.1029/2007GL031865>.
- Barnes, R. (2016). Parallel priority-flood depression filling for trillion cell digital elevation models on desktops or clusters. *Computers & Geosciences*, *96*, 56-68. <http://dx.doi.org/10.1016/j.cageo.2016.07.001>.
- Barnes, R. (2017). Parallel non-divergent flow accumulation for trillion cell digital elevation models on desktops or clusters. *Environmental Modelling & Software*, *92*, 202-212. <http://dx.doi.org/10.1016/j.envsoft.2017.02.022>.
- Barnes, R. (2018). RichDEM: high-performance terrain analysis. *PeerJ*, <http://dx.doi.org/10.7287/peerj.preprints.27099v1>.
- Barnes, R., Lehman, C., & Mulla, D. (2014a). An efficient assignment of drainage direction over flat surfaces in raster digital elevation models. *Computers & Geosciences*, *62*, 128-135. <http://dx.doi.org/10.1016/j.cageo.2013.01.009>.
- Barnes, R., Lehman, C., & Mulla, D. (2014b). Priority-flood: an optimal depression-filling and watershed-labeling algorithm for digital elevation models. *Computers & Geosciences*, *62*, 117-127. <http://dx.doi.org/10.1016/j.cageo.2013.04.024>.
- Barnes, R., Lehman, C., & Mulla, D. (2016). Distributed parallel D8 up-slope area calculation in digital elevation models. *arXiv*, 1605.05773. <http://dx.doi.org/10.48550/ARXIV.1605.05773>.
- Bigdeli, B., Amini Amirkolaei, H., & Pahlavani, P. (2018). DTM extraction under forest canopy using LiDAR data and a modified invasive weed optimization algorithm. *Remote Sensing of Environment*, *216*, 289-300. <http://dx.doi.org/10.1016/j.rse.2018.06.045>.
- Buarque, D. C., Fan, F. M., Paz, A. R., & Collischonn, W. (2009). Comparação de métodos para definir direções de escoamento a partir de modelos digitais de elevação. *RBRH*, *14*(2), 91-103. <http://dx.doi.org/10.21168/rbrh.v14n2.p91-103>.
- Chen, C., Jin, A., Yang, B., Ma, R., Sun, S., Wang, Z., Zong, Z., & Zhang, F. (2022a). DCPLD-Net: a diffusion coupled convolution neural network for real-time power transmission lines detection from UAV-Borne LiDAR data. *International Journal of Applied Earth Observation and Geoinformation*, *112*, 102960. <http://dx.doi.org/10.1016/j.jag.2022.102960>.
- Chen, Z., Deng, L., Luo, Y., Li, D., Marcato Junior, J., Nunes Gonçalves, W., Awal Md Nurunnabi, A., Li, J., Wang, C., & Li, D. (2022b). Road extraction in remote sensing data: a survey. *International Journal of Applied Earth Observation and Geoinformation*, *112*, 102833. <http://dx.doi.org/10.1016/j.jag.2022.102833>.
- Choi, Y., Yi, H., & Park, H.-D. (2011). A new algorithm for grid-based hydrologic analysis by incorporating stormwater infrastructure. *Computers & Geosciences*, *37*(8), 1035-1044. <http://dx.doi.org/10.1016/j.cageo.2010.07.008>.
- Cirilo, J. A., & Alves, F. H. B. (2014). Suporte de informações georreferenciadas de alta resolução para implantação de infraestrutura e planejamento territorial. *Revista Brasileira de Geografia Física*, *7*, 9.
- Cirilo, J. A., Alves, F. H. B., Silva, B. M., & Campos, P. H. A. L. C. (2015). Pernambuco tridimensional: base de dados espaciais para planejamento urbano e gestão territorial. In *12th Simpósio de Hidráulica e Recursos Hídricos dos Países de Expressão Portuguesa*, Brasília. Retrieved in 2022, November 14, from <https://anais.abrhidro.org.br/job.php?job=12751>
- Dalagnol, R., Wagner, F. H., Galvão, L. S., Streher, A. S., Phillips, O. L., Gloor, E., Pugh, T. A. M., Ometto, J. P. H. B., & Aragão, L. E. O. C. (2021). Large-scale variations in the dynamics of Amazon forest canopy gaps from airborne lidar data and opportunities for tree mortality estimates. *Scientific Reports*, *11*(1), 1388. PMID:33446809. <http://dx.doi.org/10.1038/s41598-020-80809-w>.
- Detto, M., Asner, G. P., Muller-Landau, H. C., & Sonnentag, O. (2015). Spatial variability in tropical forest leaf area density from multireturn lidar and modeling: Multireturn LiDAR and Tropical Forest. *Journal of Geophysical Research: Biogeosciences*, *120*(2), 294-309. <http://dx.doi.org/10.1002/2014JG002774>.
- Döll, P., & Lehner, B. (2002). Validation of a new global 30-min drainage direction map. *Journal of Hydrology*, *258*(1-4), 214-231. [http://dx.doi.org/10.1016/S0022-1694\(01\)00565-0](http://dx.doi.org/10.1016/S0022-1694(01)00565-0).
- Dong, P., & Chen, Q. (2018). *LiDAR remote sensing and applications*. Boca Raton: Taylor & Francis.
- Du, C., Ye, A., Gan, Y., You, J., Duan, Q., Ma, F., & Hou, J. (2017). Drainage network extraction from a high-resolution DEM using parallel programming in the NET Framework. *Journal of Hydrology*, *555*, 506-517. <http://dx.doi.org/10.1016/j.jhydrol.2017.10.034>.
- Duke, G. D., Kienzle, S. W., Johnson, D. L., & Byrne, J. M. (2006). Incorporating ancillary data to refine anthropogenically modified overland flow paths. *Hydrological Processes*, *20*(8), 1827-1843. <http://dx.doi.org/10.1002/hyp.5964>.
- Erdbrügger, J., van Meerveld, I., Bishop, K., & Seibert, J. (2021). Effect of DEM-smoothing and -aggregation on topographically-based flow directions and catchment boundaries. *Journal of Hydrology*, *602*, 126717. <http://dx.doi.org/10.1016/j.jhydrol.2021.126717>.
- Farr, T. G., Rosen, P. A., Caro, E., Crippen, R., Duren, R., Hensley, S., Kobrick, M., Paller, M., Rodriguez, E., Roth, L., Seal, D., Shaffer, S., Shimada, J., Umland, J., Werner, M., Oskin, M., Burbank, D., & Alsdorf, D. (2007). The Shuttle Radar Topography Mission. *Reviews of Geophysics*, *45*(2), RG2004. <http://dx.doi.org/10.1029/2005RG000183>.
- Fekete, B. M., Vörösmarty, C. J., & Lammers, R. B. (2001). Scaling gridded river networks for macroscale hydrology: Development, analysis, and control of error. *Water Resources Research*, *37*(7), 1955-1967. <http://dx.doi.org/10.1029/2001WR900024>.

- Gandolfi, C., & Bischetti, G. B. (1997). Influence of the drainage network identification method on geomorphological properties and hydrological response. *Hydrological Processes*, 11(4), 353-375. [http://dx.doi.org/10.1002/\(SICI\)1099-1085\(19970330\)11:4<353::AID-HYP436>3.0.CO;2-L](http://dx.doi.org/10.1002/(SICI)1099-1085(19970330)11:4<353::AID-HYP436>3.0.CO;2-L).
- Gatzolis, D., & Fried, J. S. (2004). Adding Gaussian noise to inaccurate digital elevation models improves spatial fidelity of derived drainage networks: adding gaussian noise to inaccurate dem. *Water Resources Research*, 40(2), <http://dx.doi.org/10.1029/2002WR001735>.
- Getirana, A. C. V., Bonnet, M.-P., Rotunno Filho, O. C., & Mansur, W. J. (2009). Improving hydrological information acquisition from DEM processing in floodplains. *Hydrological Processes*, 23(3), 502-514. <http://dx.doi.org/10.1002/hyp.7167>.
- Giannoni, F., Roth, G., & Rudari, R. (2005). A procedure for drainage network identification from geomorphology and its application to the prediction of the hydrologic response. *Advances in Water Resources*, 28(6), 567-581. <http://dx.doi.org/10.1016/j.advwatres.2004.11.013>.
- Gironás, J., Niemann, J. D., Roesner, L. A., Rodriguez, F., & Andrieu, H. (2010). Evaluation of Methods for Representing Urban Terrain in Storm-Water Modeling. *Journal of Hydrologic Engineering*, 15(1), 1-14. [http://dx.doi.org/10.1061/\(ASCE\)HE.1943-5584.0000142](http://dx.doi.org/10.1061/(ASCE)HE.1943-5584.0000142).
- Gökgöz, T., & Baker, M. (2015). Large scale landform mapping using Lidar DEM. *ISPRS International Journal of Geo-Information*, 4(3), 1336-1345. <http://dx.doi.org/10.3390/ijgi4031336>.
- Gong, J., & Xie, J. (2009). Extraction of drainage networks from large terrain datasets using high throughput computing. *Computers & Geosciences*, 35(2), 337-346. <http://dx.doi.org/10.1016/j.cageo.2008.09.002>.
- Grohmann, C. H. (2018). Evaluation of TanDEM-X DEMs on selected Brazilian sites: comparison with SRTM, ASTER GDEM and ALOS AW3D30. *Remote Sensing of Environment*, 212, 121-133. <http://dx.doi.org/10.1016/j.rse.2018.04.043>.
- Hawker, L., Bates, P., Neal, J., & Rougier, J. (2018). Perspectives on Digital Elevation Model (DEM) simulation for flood modeling in the absence of a high-accuracy open access global DEM. *Frontiers in Earth Science*, 6, 233. <http://dx.doi.org/10.3389/feart.2018.00233>.
- Hawker, L., Uhe, P., Paulo, L., Sosa, J., Savage, J., Sampson, C., & Neal, J. (2022). A 30 m global map of elevation with forests and buildings removed. *Environmental Research Letters*, 17(2), 024016. <http://dx.doi.org/10.1088/1748-9326/ac4d4f>.
- Höfle, B., & Rutzinger, M. (2011). Topographic airborne LiDAR in geomorphology: a technological perspective. *Zeitschrift Für Geomorphologie*. *Zeitschrift für Geomorphologie*, 55(2), 1-29. <http://dx.doi.org/10.1127/0372-8854/2011/0055S2-0043>.
- Instituto de Tecnologia de Pernambuco – ITEP. (2018a). *Pernambuco Tridimensional – PE 3D: validação dos produtos aerofotogramétricos e perfilamento a laser – Relatório final do Bloco 1—análise de consistência lógica, completude e exatidão posicional* (No. 1, 578 p). Recife: ITEP.
- Instituto de Tecnologia de Pernambuco – ITEP. (2018b). *Pernambuco Tridimensional – PE 3D: validação dos produtos aerofotogramétricos e perfilamento a laser – Relatório final do Bloco 2—análise de consistência lógica e completude* (No. 2, 549 p). Recife: ITEP.
- Jamali, B., Löwe, R., Bach, P. M., Urich, C., Arnbjerg-Nielsen, K., & Deletic, A. (2018). A rapid urban flood inundation and damage assessment model. *Journal of Hydrology*, 564, 1085-1098. <http://dx.doi.org/10.1016/j.jhydrol.2018.07.064>.
- Jensen, J. R. (2009). *Sensoriamento remoto do ambiente: uma perspectiva em recursos terrestres* (2ª ed.). São José dos Campos: Parêntese.
- Jensen, J. R., & Epiphany, J. C. N. (2011). *Sensoriamento remoto do ambiente: uma perspectiva em recursos terrestres*. São José dos Campos: Parêntese.
- Jenson, S., & Domingue, J. (1988). Extracting topographic structure from digital elevation data for geographic information system analysis. *Photogrammetric Engineering and Remote Sensing*, 54, 1593-1600.
- Käser, D., Graf, T., Cochand, F., McLaren, R., Therrien, R., & Brunner, P. (2014). Channel representation in physically based models coupling groundwater and surface water: pitfalls and how to avoid them. *Ground Water*, 52(6), 827-836. PMID:24417289. <http://dx.doi.org/10.1111/gwat.12143>.
- Kenward, T. (2000). Effects of digital elevation model accuracy on hydrologic predictions. *Remote Sensing of Environment*, 74(3), 432-444. [http://dx.doi.org/10.1016/S0034-4257\(00\)00136-X](http://dx.doi.org/10.1016/S0034-4257(00)00136-X).
- Klein, I., Oppelt, N., & Kuenzer, C. (2021). Application of remote sensing data for locust research and management: a review. *Insects*, 12(3), 233. PMID:33803360. <http://dx.doi.org/10.3390/insects12030233>.
- Krieger, G., Moreira, A., Fiedler, H., Hajnsek, I., Werner, M., Younis, M., & Zink, M. (2007). TanDEM-X: a satellite formation for high-resolution SAR interferometry. *IEEE Transactions on Geoscience and Remote Sensing*, 45(11), 3317-3341. <http://dx.doi.org/10.1109/TGRS.2007.900693>.
- Lai, Z., Li, S., Lv, G., Pan, Z., & Fei, G. (2016). Watershed delineation using hydrographic features and a DEM in plain river network region: Watershed Delineation in Plain River Network Region. *Hydrological Processes*, 30(2), 276-288. <http://dx.doi.org/10.1002/hyp.10612>.
- Lakshmi, V., Fayne, J., & Bolten, J. (2018). A comparative study of available water in the major river basins of the world. *Journal of Hydrology*, 567, 510-532. PMID:32020949. <http://dx.doi.org/10.1016/j.jhydrol.2018.10.038>.
- Lauri, H., & Kumm, M. (2014). Improving the accuracy of a grid-based distributed hydrological model using slope and river length

- corrections in a large river basin: case Mekong. *Nordic Hydrology*, 45(4–5), 715–726. <http://dx.doi.org/10.2166/nh.2013.238>.
- Lecours, V., Devillers, R., Simms, A. E., Lucieer, V. L., & Brown, C. J. (2017). Towards a framework for terrain attribute selection in environmental studies. *Environmental Modelling & Software*, 89, 19–30. <http://dx.doi.org/10.1016/j.envsoft.2016.11.027>.
- Li, H., Zhao, J., Yan, B., Yue, L., & Wang, L. (2022). Global DEMs vary from one to another: an evaluation of newly released Copernicus, NASA and AW3D30 DEM on selected terrains of China using ICESat-2 altimetry data. *International Journal of Digital Earth*, 15(1), 1149–1168. <http://dx.doi.org/10.1080/17538947.2022.2094002>.
- Li, T. J. (2009). Modeling the process of hillslope soil erosion in the Loess Plateau. *Journal of Environmental Informatics*, 14(1), 1–10. <http://dx.doi.org/10.3808/jei.200900148>.
- Lillesand, T. M., Kiefer, R. W., & Chipman, J. W. (2015). *Remote sensing and image interpretation* (7th ed). New York: Wiley.
- Lindsay, J. B. (2016). The practice of DEM stream burning revisited. *Earth Surface Processes and Landforms*, 41(5), 658–668. <http://dx.doi.org/10.1002/esp.3888>.
- Lindsay, J. B., & Dhun, K. (2015). Modelling surface drainage patterns in altered landscapes using LiDAR. *International Journal of Geographical Information Science*, 29(3), 397–411. <http://dx.doi.org/10.1080/13658816.2014.975715>.
- Lindsay, J. B., & Evans, M. G. (2008). The influence of elevation error on the morphometrics of channel networks extracted from DEMs and the implications for hydrological modelling. *Hydrological Processes*, 22(11), 1588–1603. <http://dx.doi.org/10.1002/hyp.6728>.
- Lindsay, J. B., Francioni, A., & Cockburn, J. M. H. (2019). LiDAR DEM smoothing and the preservation of drainage features. *Remote Sensing*, 11(16), 1926. <http://dx.doi.org/10.3390/rs11161926>.
- Maidment, D. R. (2017). Conceptual Framework for the National Flood Interoperability Experiment. *Journal of the American Water Resources Association*, 53(2), 245–257. <http://dx.doi.org/10.1111/1752-1688.12474>.
- Marks, D., Dozier, J., & Frew, J. (1984). Automated basin delineation from digital elevation data. *Geo-Processing*, 2, 299–311.
- Maté-González, M. Á., Sánchez-Aparicio, L. J., Sáez Blázquez, C., Carrasco García, P., Álvarez-Alonso, D., de Andrés-Herrero, M., García-Davalillo, J. C., González-Aguilera, D., Hernández Ruiz, M., Jordá Bordehore, L., López Carnicero, C., & Mora, R. (2019). On the combination of remote sensing and geophysical methods for the digitalization of the San Lázaro Middle Paleolithic Rock Shelter (Segovia, Central Iberia, Spain). *Remote Sensing*, 11(17), 2035. <http://dx.doi.org/10.3390/rs11172035>.
- Mayorga, E., Aufdenkampe, A. K., Masiello, C. A., Krusche, A. V., Hedges, J. I., Quay, P. D., Richey, J. E., & Brown, T. A. (2005). Young organic matter as a source of carbon dioxide outgassing from Amazonian rivers. *Nature*, 436(7050), 538–541. PMID:16049484. <http://dx.doi.org/10.1038/nature03880>.
- McCabe, M. F., Rodell, M., Alsdorf, D. E., Miralles, D. G., Uijlenhoet, R., Wagner, W., Lucieer, A., Houborg, R., Verhoest, N. E. C., Franz, T. E., Shi, J., Gao, H., & Wood, E. F. (2017). The future of Earth observation in hydrology. *Hydrology and Earth System Sciences*, 21(7), 3879–3914. PMID:30233123. <http://dx.doi.org/10.5194/hess-21-3879-2017>.
- Moretti, G., & Orlandini, S. (2018). Hydrography-Driven Coarsening of Grid Digital Elevation Models. *Water Resources Research*, 54(5), 3654–3672. <http://dx.doi.org/10.1029/2017WR021206>.
- Mukherjee, S., Joshi, P. K., Mukherjee, S., Ghosh, A., Garg, R. D., & Mukhopadhyay, A. (2013). Evaluation of vertical accuracy of open source Digital Elevation Model (DEM). *International Journal of Applied Earth Observation and Geoinformation*, 21, 205–217. <http://dx.doi.org/10.1016/j.jag.2012.09.004>.
- Munoth, P., & Goyal, R. (2019). Effects of DEM source, spatial resolution and drainage area threshold values on hydrological modeling. *Water Resources Management*, 33(9), 3303–3319. <http://dx.doi.org/10.1007/s11269-019-02303-x>.
- Murphy, P. N. C., Ogilvie, J., Meng, F.-R., & Arp, P. (2008). Stream network modelling using lidar and photogrammetric digital elevation models: A comparison and field verification. *Hydrological Processes*, 22(12), 1747–1754. <http://dx.doi.org/10.1002/hyp.6770>.
- Murray, N. J., Keith, D. A., Simpson, D., Wilshire, J. H., & Lucas, R. M. (2018). REMAP: an online remote sensing application for land cover classification and monitoring. *Methods in Ecology and Evolution*, 9(9), 2019–2027. <http://dx.doi.org/10.1111/2041-210X.13043>.
- Ngula Niipele, J., & Chen, J. (2019). The usefulness of alos-palsar dem data for drainage extraction in semi-arid environments in The Iishana sub-basin. *Journal of Hydrology. Regional Studies*, 21, 57–67. <http://dx.doi.org/10.1016/j.ejrh.2018.11.003>.
- Nikolakopoulos, K. G., Choussiafis, C., & Karathanassi, V. (2015). Assessing the quality of DSM from ALOS optical and radar data for automatic drainage extraction. *Earth Science Informatics*, 8(2), 293–307. <http://dx.doi.org/10.1007/s12145-014-0199-6>.
- Noh, S. J., Lee, J.-H., Lee, S., Kawaike, K., & Seo, D.-J. (2018). Hyper-resolution 1D-2D urban flood modelling using LiDAR data and hybrid parallelization. *Environmental Modelling & Software*, 103, 131–145. <http://dx.doi.org/10.1016/j.envsoft.2018.02.008>.
- Novo, E. M. L. M. (2010). *Sensoriamento remoto: princípios e aplicações* (4ª ed. rev). São Paulo: Blucher.
- O’Callaghan, J. F., & Mark, D. M. (1984). The extraction of drainage networks from digital elevation data. *Computer Vision Graphics and Image Processing*, 28(3), 323–344. [http://dx.doi.org/10.1016/S0734-189X\(84\)80011-0](http://dx.doi.org/10.1016/S0734-189X(84)80011-0).

- O'Loughlin, F. E., Paiva, R. C. D., Durand, M., Alsdorf, D. E., & Bates, P. D. (2016). A multi-sensor approach towards a global vegetation corrected SRTM DEM product. *Remote Sensing of Environment*, 182, 49-59. <http://dx.doi.org/10.1016/j.rse.2016.04.018>.
- Olivera, F., & Raina, R. (2003). Development of large scale gridded river networks from vector stream data. *Journal of the American Water Resources Association*, 39(5), 1235-1248. <http://dx.doi.org/10.1111/j.1752-1688.2003.tb03705.x>.
- Paz, A. R., & Collischonn, W. (2008). Derivacao de rede de drenagem a partir de dados do SRTM. *Revista Geográfica Acadêmica*, 2(2), 84-95.
- Persendt, F. C., & Gomez, C. (2016). Assessment of drainage network extractions in a low-relief area of the Cuvelai Basin (Namibia) from multiple sources: LiDAR, topographic maps, and digital aerial orthophotographs. *Geomorphology*, 260, 32-50. <http://dx.doi.org/10.1016/j.geomorph.2015.06.047>.
- Pettorelli, N., Schulte to Bühne, H., Tulloch, A., Dubois, G., Macinnis-Ng, C., Queirós, A. M., Keith, D. A., Wegmann, M., Schrodt, F., Stellmes, M., Sonnenschein, R., Geller, G. N., Roy, S., Somers, B., Murray, N., Bland, L., Geijzendorffer, I., Kerr, J. T., Broszeit, S., Leitão, P. J., Duncan, C., El Serafy, G., He, K. S., Blanchard, J. L., Lucas, R., Mairota, P., Webb, T. J., & Nicholson, E. (2018). Satellite remote sensing of ecosystem functions: Opportunities, challenges and way forward. *Remote Sensing in Ecology and Conservation*, 4(2), 71-93. <http://dx.doi.org/10.1002/rse2.59>.
- Piégay, H., Hupp, C. R., Citterio, A., Dufour, S., Moulin, B., & Walling, D. E. (2008). Spatial and temporal variability in sedimentation rates associated with cutoff channel infill deposits: Ain River, France: sedimentation rates in former channel PL. *Water Resources Research*, 44(5), <http://dx.doi.org/10.1029/2006WR005260>.
- Raaflaub, L. D., & Collins, M. J. (2006). The effect of error in gridded digital elevation models on the estimation of topographic parameters. *Environmental Modelling & Software*, 21(5), 710-732. <http://dx.doi.org/10.1016/j.envsoft.2005.02.003>.
- Rabus, B., Eineder, M., Roth, A., & Bamler, R. (2003). The shuttle radar topography mission: a new class of digital elevation models acquired by spaceborne radar. *ISPRS Journal of Photogrammetry and Remote Sensing*, 57(4), 241-262. [http://dx.doi.org/10.1016/S0924-2716\(02\)00124-7](http://dx.doi.org/10.1016/S0924-2716(02)00124-7).
- Riegler, G., Hennig, S. D., & Weber, M. (2015). WORLDDEM: a novel global foundation layer. *The International Archives of the Photogrammetry, Remote Sensing and Spatial Information Sciences*, XL-3(W2), 183-187. <http://dx.doi.org/10.5194/isprsarchives-XL-3-W2-183-2015>.
- Robinson, N., Regetz, J., & Guralnick, R. P. (2014). EarthEnv-DEM90: A nearly-global, void-free, multi-scale smoothed, 90m digital elevation model from fused ASTER and SRTM data. *ISPRS Journal of Photogrammetry and Remote Sensing*, 87, 57-67. <http://dx.doi.org/10.1016/j.isprsjprs.2013.11.002>.
- Roelens, J., Rosier, I., Dondeyne, S., Van Orshoven, J., & Diels, J. (2018). Extracting drainage networks and their connectivity using LiDAR data. *Hydrological Processes*, 32(8), 1026-1037. <http://dx.doi.org/10.1002/hyp.11472>.
- Sanders, B. F. (2007). Evaluation of on-line DEMs for flood inundation modeling. *Advances in Water Resources*, 30(8), 1831-1843. <http://dx.doi.org/10.1016/j.advwatres.2007.02.005>.
- Saraiva, A. G. S., & Paz, A. R. (2014). Multi-step change of scale approach for deriving coarse-resolution flow directions. *Computers & Geosciences*, 68, 53-63. <http://dx.doi.org/10.1016/j.cageo.2014.04.002>.
- Schulz, W. H., Coe, J. A., Ricci, P. P., Smoczyk, G. M., Shurtleff, B. L., & Panosky, J. (2017). Landslide kinematics and their potential controls from hourly to decadal timescales: insights from integrating ground-based InSAR measurements with structural maps and long-term monitoring data. *Geomorphology*, 285, 121-136. <http://dx.doi.org/10.1016/j.geomorph.2017.02.011>.
- Schumann, G. J.-P., & Bates, P. D. (2018). The need for a high-accuracy, open-access global DEM. *Frontiers in Earth Science*, 6, 225. <http://dx.doi.org/10.3389/feart.2018.00225>.
- Sedgewick, R. (1992). *Algorithms in C++* (1st ed). Reading: Addison-Wesley.
- Semenova, O., & Beven, K. (2015). Barriers to progress in distributed hydrological modelling. *Hydrological Processes*, 29(8), 2074-2078. <http://dx.doi.org/10.1002/hyp.10434>.
- Siqueira, V., Fleischmann, A., Jardim, P., Fan, F., & Collischonn, W. (2016). IPH-Hydro Tools: A GIS coupled tool for watershed topology acquisition in an open-source environment. *RBRH*, 21(1), 274-287. <http://dx.doi.org/10.21168/rbrh.v21n1.p274-287>.
- Smith, M. J., & Clark, C. D. (2005). Methods for the visualization of digital elevation models for landform mapping. *Earth Surface Processes and Landforms*, 30(7), 885-900. <http://dx.doi.org/10.1002/esp.1210>.
- Sofia, G., Fontana, G. D., & Tarolli, P. (2014). High-resolution topography and anthropogenic feature extraction: testing geomorphometric parameters in floodplains: LiDAR DTM and anthropogenic feature extraction. *Hydrological Processes*, 28(4), 2046-2061. <http://dx.doi.org/10.1002/hyp.9727>.
- Sousa, T. M. I., & Paz, A. R. (2017). How to evaluate the quality of coarse-resolution DEM-derived drainage networks. *Hydrological Processes*, 31(19), 3379-3395. <http://dx.doi.org/10.1002/hyp.11262>.
- Stanislawski, L. V., Survila, K., Wendel, J., Liu, Y., & Buttenfield, B. P. (2018). An open source high-performance solution to extract surface water drainage networks from diverse terrain conditions. *Cartography and Geographic Information Science*, 45(4), 319-328. <http://dx.doi.org/10.1080/15230406.2017.1337524>.
- Syvitski, J. P. M., & Milliman, J. D. (2007). Geology, geography, and humans battle for dominance over the delivery of fluvial sediment to the Coastal Ocean. *The Journal of Geology*, 115(1), 1-19. <http://dx.doi.org/10.1086/509246>.
- Tachikawa, T., Hato, M., Kaku, M., & Iwasaki, A. (2011). Characteristics of ASTER GDEM version 2. In *2011 IEEE International Geoscience and Remote Sensing Symposium* (pp. 3657-3660), Vancouver, BC, Canada. <http://dx.doi.org/10.1109/IGARSS.2011.6050017>.

- Tadono, T., Takaku, J., Tsutsui, K., Oda, F., & Nagai, H. (2015). Status of ALOS World 3D (AW3D) global DSM generation. In *2015 IEEE International Geoscience and Remote Sensing Symposium (IGARSS)* (pp. 3822-3825), Milan, Italy. <http://dx.doi.org/10.1109/IGARSS.2015.7326657>.
- Takaku, J., Tadono, T., & Tsutsui, K. (2014). Generation of high resolution global DSM from ALOS PRISM. *The International Archives of the Photogrammetry, Remote Sensing and Spatial Information Sciences*, *XL-4*, 243-248. <http://dx.doi.org/10.5194/isprsarchives-XL-4-243-2014>.
- Torre-Tojal, L., Bastarrika, A., Boyano, A., Lopez-Guede, J. M., & Graña, M. (2022). Above-ground biomass estimation from LiDAR data using random forest algorithms. *Journal of Computational Science*, *58*, 101517. <http://dx.doi.org/10.1016/j.jocs.2021.101517>.
- Trepkli, K., Balstrøm, T., Friberg, T., Fog, B., Allotey, A. N., Kofie, R. Y., & Møller-Jensen, L. (2022). UAV-borne, LiDAR-based elevation modelling: a method for improving local-scale urban flood risk assessment. *Natural Hazards*, *113*(1), 423-451. <http://dx.doi.org/10.1007/s11069-022-05308-9>.
- van Leeuwen, M., & Nieuwenhuis, M. (2010). Retrieval of forest structural parameters using LiDAR remote sensing. *European Journal of Forest Research*, *129*(4), 749-770. <http://dx.doi.org/10.1007/s10342-010-0381-4>.
- Wang, C., & Glenn, N. F. (2008). A linear regression method for tree canopy height estimation using airborne lidar data. *Canadian Journal of Remote Sensing*, *34*(Suppl. 2), S217-S227. <http://dx.doi.org/10.5589/m08-043>.
- Wang, L., & Liu, H. (2006). An efficient method for identifying and filling surface depressions in digital elevation models for hydrologic analysis and modelling. *International Journal of Geographical Information Science*, *20*(2), 193-213. <http://dx.doi.org/10.1080/13658810500433453>.
- Wang, N., Shi, Z., & Zhang, Z. (2022). Road boundary, curb and surface extraction from 3D mobile LiDAR point clouds in urban environment. *Canadian Journal of Remote Sensing*, *48*(4), 504-519. <http://dx.doi.org/10.1080/07038992.2022.2096579>.
- Woodrow, K., Lindsay, J. B., & Berg, A. A. (2016). Evaluating DEM conditioning techniques, elevation source data, and grid resolution for field-scale hydrological parameter extraction. *Journal of Hydrology*, *540*, 1022-1029. <http://dx.doi.org/10.1016/j.jhydrol.2016.07.018>.
- Wu, S., Li, J., & Huang, G. H. (2008). A study on DEM-derived primary topographic attributes for hydrologic applications: sensitivity to elevation data resolution. *Applied Geography (Sevenoaks, England)*, *28*(3), 210-223. <http://dx.doi.org/10.1016/j.apgeog.2008.02.006>.
- Xiang, M., Li, Y., Yang, J., Li, Y., Li, F., Hu, B., & Cao, Y. (2020). Assessment of heavy metal pollution in soil and classification of pollution risk management and control zones in the industrial developed city. *Environmental Management*, *66*(6), 1105-1119. PMID:33070200. <http://dx.doi.org/10.1007/s00267-020-01370-w>.
- Yamazaki, D., Ikeshima, D., Sosa, J., Bates, P. D., Allen, G. H., & Pavelsky, T. M. (2019). MERIT hydro: a high-resolution global hydrography map based on latest topography dataset. *Water Resources Research*, *55*(6), 5053-5073. <http://dx.doi.org/10.1029/2019WR024873>.
- Yamazaki, D., Oki, T., & Kanae, S. (2009). Deriving a global river network map and its sub-grid topographic characteristics from a fine-resolution flow direction map. *Hydrology and Earth System Sciences*, *13*(11), 2241-2251. <http://dx.doi.org/10.5194/hess-13-2241-2009>.
- Yang, P., Ames, D. P., Fonseca, A., Anderson, D., Shrestha, R., Glenn, N. F., & Cao, Y. (2014). What is the effect of LiDAR-derived DEM resolution on large-scale watershed model results? *Environmental Modelling & Software*, *58*, 48-57. <http://dx.doi.org/10.1016/j.envsoft.2014.04.005>.
- Yıldırım, A. A., Watson, D., Tarboton, D., & Wallace, R. M. (2015). A virtual tile approach to raster-based calculations of large digital elevation models in a shared-memory system. *Computers & Geosciences*, *82*, 78-88. <http://dx.doi.org/10.1016/j.cageo.2015.05.014>.
- Zhang, X., Meng, X., Li, C., Shang, N., Wang, J., Xu, Y., Wu, T., & Mugnier, C. (2021). Micro-topography mapping through terrestrial LiDAR in densely vegetated coastal environments. *ISPRS International Journal of Geo-Information*, *10*(10), 665. <http://dx.doi.org/10.3390/ijgi10100665>.
- Zhou, G., Wei, H., & Fu, S. (2019). A fast and simple algorithm for calculating flow accumulation matrices from raster digital elevation. *Frontiers of Earth Science*, *13*(2), 317-326. <http://dx.doi.org/10.1007/s11707-018-0725-9>.
- Zhu, Q., Tian, Y., & Zhao, J. (2006). An efficient depression processing algorithm for hydrologic analysis. *Computers & Geosciences*, *32*(5), 615-623. <http://dx.doi.org/10.1016/j.cageo.2005.09.001>.
- Zováthi, Ö., Nagy, B., & Benedek, C. (2022). Point cloud registration and change detection in urban environment using an onboard Lidar sensor and MLS reference data. *International Journal of Applied Earth Observation and Geoinformation*, *110*, 102767. <http://dx.doi.org/10.1016/j.jag.2022.102767>.

Authors contributions

Rafael Lopes Mendonça: Literature review, data collection, study design, methodology development and application, results discussion and paper writing.

Adriano Rolim da Paz: Study design, results discussion and paper writing

Editor-in-Chief: Adilson Pinheiro

Associated Editor: Fernando Mainardi Fan